Scaling between cell cycle duration and wing growth is regulated by Fat-Dachsous signaling in *Drosophila*

Andrew Liu[1,2], Jessica O'Connell[1], Farley Wall[1], and Richard W. Carthew[1,2,*]

1. Department of Molecular Biosciences, Northwestern University, Evanston IL
2. NSF-Simons Center for Quantitative Biology, Northwestern University, Evanston IL

* Corresponding author (r-carthew@northwestern.edu)

Abstract

The atypical cadherins Fat and Dachsous (Ds) signal through the Hippo pathway to regulate growth of numerous organs, including the *Drosophila* wing. Here, we find that Ds-Fat signaling tunes a unique feature of cell proliferation found to control the rate of wing growth. The duration of the cell cycle increases in direct proportion to the size of the wing, leading to linear rather than exponential growth. Ds-Fat signaling enhances the rate at which the cell cycle lengthens with wing size, thus diminishing the linear rate of wing growth. We show that this results in a complex but stereotyped relative scaling of wing growth with body growth in *Drosophila*. Finally, we examine the dynamics of Fat and Ds protein distribution in the wing, observing graded distributions that change during growth. However, the significance of these dynamics is unclear since perturbations in expression have negligible impact on wing growth.

Introduction

A fundamental aspect of animal development is growth. At the organismal level, growth is coupled with morphogenesis and development, and can also be separated into stages with physical constraints (e.g., molting events). At the organ level, growth is coupled with body growth to ensure relative scaling for proper form and function. At the cellular level, growth is interpreted as the decision to divide or not and to increase in size or not. These three levels of growth are integrated with one another to ensure that cells make appropriate growth choices based on feedback from the other two levels.

Growth of the body and its organs are controlled in two ways. The rate of growth over time is internally regulated with an upper limit set independent of such environmental factors as nutrition (Conlon and Raff, 1999). The size setpoint when growth ceases is also internally controlled (Leevers and McNeill, 2005). Typically, the setpoint is reached when the animal transitions to adulthood. The two control processes are linked with one another. For example, *Drosophila* that are deficient in insulin signaling grow slowly and their final size setpoint is smaller than normal (Rulifson et al., 2002). However, sometimes the growth-arrest process compensates for an abnormal growth rate to generate a normal size setpoint (Leevers and McNeill, 2005; Penzo-Mendez and Stanger, 2015).

The wing of *Drosophila* is a well-established model system to study organ growth control. In *Drosophila* larvae, the anlage fated to form the adult wing blade is composed of an epithelial domain embedded within a larger epithelial sheet named the wing imaginal disc or wing disc (Fig. 1A). The anlage, called a wing pouch, is surrounded by wing disc cells that will form the wing hinge and notum, which is the dorsal thorax. Two wing discs reside within the body cavity of a larva (Fig. 1A), and they grow in size as the larva undergoes three successive molts. Wing discs uniformly grow by asynchronous cell division until the animal undergoes the final molt at the end of its third larval instar stage and pupates (Bryant and Levinson, 1985;

81 Neto-Silva et al., 2009). During pupation, each wing pouch develops into a single adult wing
82 blade.

83 Growth control of the wing disc operates through several mechanisms (Nijhout and
84 Callier, 2015). Hormones such as insulin-like peptides and ecdysone coordinate wing growth
85 with environmental inputs such as nutrition and molting events (Colombani et al., 2005).
86 Paracrine growth factors are secreted from a subset of wing disc cells and are transported
87 through the disc tissue to stimulate cell proliferation (Baena-Lopez et al., 2012). The BMP
88 morphogen Decapentaplegic (Dpp) and Wnt morphogen Wingless (Wg) are two such growth
89 factors.

90 Another signal transduction pathway - the Hippo pathway - also operates to regulate
91 growth of the wing disc (Pan, 2010; Boggiano and Fehon, 2012). The Hippo pathway is
92 controlled by two different signals, both of which are locally transmitted. Mechanical stress from
93 local tissue compression caused by differential growth alters the cytoskeletal tension in wing
94 disc cells, which in turn regulates the Hippo pathway (Legoff et al., 2013; Rauskolb et al., 2014;
95 Pan et al., 2016). Increased tension inactivates the Warts kinase, leading to upregulation of the
96 Yorkie (Yki) transcription factor and growth promotion. A second signal that modulates the
97 Hippo pathway in wing disc cells is mediated by two atypical cadherin molecules, Fat and
98 Dachsous (Ds) (Pan, 2010). Ds and Fat are growth inhibitory factors. The two proteins bind to
99 one another on opposing cell membranes at adherens junctions, and Ds is thought to be a
100 ligand for Fat in many circumstances (Clark et al., 1995; Ma et al., 2003; Matakatsu and Blair,
101 2004). However, Ds has receptor-like properties as well (Matakatsu and Blair, 2006). Binding of
102 Fat and Ds is also modulated by the kinase Four-jointed (Fj) (Ishikawa et al., 2008). When Fat is
103 activated, it induces the destruction of an unconventional myosin called Dachs (Cho et al., 2006;
104 Mao et al., 2006; Rogulja et al., 2008; Zhang et al., 2016).This derepresses Warts, which then
105 inhibits Yki from transcribing growth-promoting genes (Cho et al., 2006; Vrabioiu and Struhl,

106 2015). A prevailing model for Ds signaling to Fat is not via its absolute concentration but by the
107 steepness of its local concentration gradient (Pan, 2010). Ds is expressed across the wing
108 pouch in a graded fashion, and if the gradient is steep, growth is stimulated whereas if the
109 gradient is shallow, growth is inhibited (Rogulja et al., 2008; Willecke et al., 2008).

110 Various molecular models for wing growth control have been developed in detail.
111 However, what is unresolved are explanations for how these molecular mechanisms regulate
112 the macroscopic features of growth. Namely, how do the molecular mechanisms regulate
113 growth of the different domains of the wing disc: wing pouch, hinge, notum. How do they
114 regulate the relative scaling of the wing to the body as both are growing in size. How do the
115 different molecular mechanisms precisely regulate the two key growth control processes: growth
116 rate and growth arrest.

117 Here, we focus on Ds-Fat signaling and address these questions with the aim of
118 connecting the molecular perspective of growth control to a more macroscopic perspective. We
119 find that Ds-Fat signaling tunes a unique feature of cell proliferation found to control the rate of
120 wing pouch growth. The duration of the cell cycle increases in direct proportion to the size of the
121 wing pouch, leading to linear rather than exponential growth. Ds-Fat signaling enhances the rate
122 at which the cell cycle lengthens with wing size, thus diminishing the linear rate of wing growth.
123 Duration of the cell cycle is coupled to relative change in Dpp signaling over time (Wartlick et al.,
124 2011), suggesting that Ds-Fat signaling increases cell sensitivity to fold-changes in Dpp over
125 time. We show that this results in a complex but stereotyped relative scaling of wing growth with
126 body growth in *Drosophila*. Finally, we examine the dynamics of Fat and Ds protein distribution
127 in the wing pouch, observing graded distributions that change during growth. However, the
128 significance of these dynamics is unclear since perturbations in expression have negligible
129 impact on wing growth.

130

Results

Quantitative properties of *Drosophila* larval wing growth

Organ growth in animals is coupled to body growth in complex ways that are specific for both the organ and species (Huxley and Teissier, 1936). We first sought to determine the relationship between growth of the wing and body in *Drosophila melanogaster*. Although previous work has studied this relationship, none have provided a quantitative description of it. Therefore, we measured body size by both wet weight and volume, while we measured wing pouch size by its volume. As expected, measurements of body weight and body volume showed a strong correlation (Fig. 1 - figure supplement 1). To measure wing pouch volume, we generated a 3D stack of confocal microscopic sections of the wing disc and used morphological landmarks (tissue folds) to demarcate the boundary between wing pouch and surrounding notum-hinge. We validated the efficacy of this method by comparing the landmark-defined boundary to the expression boundary of *vestigial*, a selector gene specifically expressed in wing pouch cells (Kim et al., 1996). The landmark method gave wing pouch measurements that were within 95.5% of measurements made by *vestigial* expression (Fig. 1 - figure supplement 2).

We focused our growth study on the third instar larval stage, which occurs over a two-day period. Beginning at 3.0 days after egg laying (AEL), we measured third instar larval bodies and wing discs every 12 hours until the larva-pupa molt. Larval body weight increased linearly from 3.0 to 4.0 days AEL, followed by a 12 hr period of slower growth, and thereafter weight remained constant (Fig. 1B). The time point at which larvae stopped growing (4.5 days AEL) coincided with the time at which they stopped feeding and underwent a 12 hr non-feeding stage (Slaidina et al., 2009). We also monitored weight as larvae underwent their molt into pupae. Weight remained constant during the one-hr white prepupal (WPP) stage and also one hr later at the brown prepupal (BPP) stage (Fig. 1C).

We also measured wing pouch growth. Wing pouch volume increased linearly over time during the early third instar stage and continued to grow during the non-feeding larval stage

157 (Fig. 1D). This was in contrast to body growth, which ceased at the non-feeding stage.
158 However, growth of the wing pouch ceased at the larva-pupa molt and its size remained
159 constant (Fig. 1E). A similar growth trajectory was observed for the notum-hinge although it
160 stopped growing sometime during the non-feeding stage (Fig. 1 - figure supplement 3A,B). End-
161 of-growth of the wing pouch was confirmed by phospho-histone H3 (PHH3) staining, which
162 marks mitotic cells. At larval stages, dividing cells were observed throughout the wing pouch
163 (Fig. 1 - figure supplement 4A,B), whereas at the WPP stage, dividing cells were only found in a
164 narrow zone where sensory organ precursor cells undergo two divisions to generate future
165 sensory organs (Fig. 1 - figure supplement 4C-E).

166 The scaling of organ growth relative to body growth during development is known as
167 *ontogenetic allometry*. For most animal species, allometric growth of organs follows a power law
168 (Huxley and Teissier, 1936), such that logarithmic transformation of the organ and body size
169 measurements fits a linear relationship (Fig. 1F). When the organ grows at the same rate as the
170 body, it exhibits isometric growth (Huxley and Teissier, 1936). When the organ grows at a faster
171 or slower rate than the body, it has positive or negative allometric growth, respectively (Fig. 1F).
172 Allometric organ growth in holometabolous insects such as *Drosophila* presents a special
173 problem arising from the fact that many adult organs derive from the imaginal discs, which are
174 non-functional in larvae. For this reason, there are fewer constraints on relative scaling, and
175 allometric growth is freer to deviate from simple scaling laws. For example, in the silkworm, its
176 wing disc grows linearly with its body while the larva feeds, but then continues its linear growth
177 after larvae have ceased feeding (Williams, 1980). Thus, its allometric growth has two linear
178 phases; the first is isometric and the second is positively allometric.

179 Since ontogenetic allometric growth of the *Drosophila* wing pouch has not been studied,
180 we plotted wet-weight body measurements versus wing pouch volume measurements taken
181 from different developmental stages (Fig. 1G). As with silkworms, allometric growth of the wing
182 pouch had two linear phases, both of which showed positive allometry. The inflection point was

183 the time when larvae ceased feeding. In contrast, the notum-hinge exhibited simpler linear-like
184 positive allometric growth (Fig. 1 - figure supplement 3C). Therefore, allometric growth control of
185 the wing imaginal disc appears to be composed of multiple mechanisms.
186
187 **Global gradients of Fat and Ds in the growing wing pouch**
188 One mechanism for growth control of the wing imaginal disc is through the atypical
189 cadherin proteins Fat and Ds. Both are type I transmembrane proteins with extensive numbers
190 of extracellular cadherin domains: 34 in Fat and 27 in Ds (Fig. 2A). Qualitative descriptions of *ds*
191 gene expression in the wing pouch indicate that cells transcribe the gene at different levels
192 depending upon their position in the pouch (Strutt and Strutt, 2002; Ma et al., 2003). We
193 confirmed that there is graded transcription across the pouch by using single molecule
194 fluorescence in situ hybridization (smFISH) (Fig. 2 - figure supplement 1A). A previous model
195 hypothesized that this generates a Ds protein gradient across the wing pouch, and the gradient
196 regulates growth by inducing Fat polarization in cells (Pan, 2010). When the Ds gradient
197 becomes flattened, it leads to growth cessation. If correct, the model suggests that the Ds
198 protein gradient should become shallow as the wing pouch reaches its final size. To test this, we
199 used quantitative confocal microscopy to measure endogenous Ds protein tagged with GFP at
200 its carboxy-terminus (Fig. 2A). Wing discs were co-stained with antibodies directed against
201 Wingless (Wg) and Engrailed (En) proteins, which mark the wing pouch midlines (Fig. 2 - figure
202 supplement 2A,B). We measured Ds-GFP across the wing pouch, excluding peripodial signal,
203 along the two midlines to gain a Cartesian perspective of the 2D expression pattern (Fig. 2 -
204 figure supplement 2C). We focused our analysis on wing pouches taken from the third instar
205 larval stage. Beginning at 4.0 days AEL, we measured Ds-GFP in the wing pouch every 12
206 hours until the larva-pupa molt. We also measured Ds-GFP at the WPP stage of the larva-pupa
207 molt.

208 At all timepoints, there was a graded distribution of Ds-GFP along both anterior-posterior
209 (AP) and dorsal-ventral (DV) axes, high at the margins and low in the center of the pouch (Fig.
210 2C,D). The gradient was asymmetric along the AP axis, being lower at the A margin than the P
211 margin. As the pouch grew larger, the Ds gradient appeared to become progressively shallower.
212 When we normalized all of the Ds-GFP profiles to their corresponding pouch sizes, the profiles
213 along the AP axis collapsed together (Fig 2E). This occurred because the maximum and
214 minimum limits of Ds-GFP abundance were conserved as the wing pouch grew. It implies that
215 dividing cells take up intermediate scalar values from their neighbors during growth, and over
216 time the steepness of the Ds gradient diminishes. In contrast, along the DV axis the normalized
217 profiles remained distinct because both maximum and minimum limits of Ds-GFP progressively
218 diminished as the wing grew (Fig. 2F).
219 We next turned to quantitative analysis of Fat protein expression. Fat is thought to be
220 uniformly expressed in the wing pouch, though it has also been described as enriched along the
221 DV midline (Garoia et al., 2000; Mao et al., 2009). We measured endogenous Fat protein
222 tagged at its carboxy-terminus with GFP (Fig. 2A and Fig. 2 - figure supplement 2D).
223 Surprisingly, Fat-GFP had a graded distribution along both the AP and DV axes; low at the
224 margins and high in the center of the wing pouch (Fig. 2G,H). The gradient profile was opposite
225 to the one we observed for Ds-GFP. As the pouch grew in size, the Fat gradient appeared to
226 grow shallower, becoming flat along the AP axis by the WPP stage. When we normalized all of
227 the Fat-GFP profiles to their corresponding pouch sizes, the profiles did not collapse (Fig
228 2I,J). The minimum limit of Fat-GFP was conserved but the maximum limit of Fat-GFP
229 progressively diminished as the wing grew.
230 The observation of a graded distribution of Fat protein was surprising since it was
231 reported that *fat* gene transcription is uniform (Garoia et al., 2000). We confirmed this
232 observation using smFISH (Fig. 2 - figure supplement 1B). We considered the possibility that
233 the gradient is generated by a post-transcriptional mechanism. To test the idea, we expressed a

234 *fat* transgene under the control of a UAS promoter. The transgene's transcription was activated
235 by Gal4 driven under control of the *daughterless* (*da*) promoter (Fig. 2K). *da-Gal4* is uniformly
236 expressed in *Drosophila* tissues (Gilbert et al., 2006). The transgenic Fat protein was epitope
237 tagged for visualization. As a control, cells also expressed Bazooka-mCherry from a second
238 UAS transgene. We then measured the abundance of tagged Fat and Bazooka across the wing
239 pouch. Bazooka protein distribution was fairly uniform along the AP axis while Fat protein was
240 graded in a similar pattern to endogenous Fat (Fig. 2L). Thus, the Fat gradient is generated by a
241 post-transcriptional mechanism.

242 Ds is known to physically interact with Fat protein and so it was possible that the Fat
243 protein gradient was controlled by Ds. To test this, we examined Fat-GFP distribution in a *ds*
244 mutant background. The magnitude of peak Fat-GFP levels at the wing pouch center was the
245 same as wildtype but the level of Fat-GFP near the margins was abnormally high (Fig. 2M).
246 Since Ds levels are highest and most steep near the margins, perhaps Ds inhibits Fat
247 expression in a dose- or gradient-dependent manner. We also followed Fat-GFP dynamics in
248 the *ds* mutant. We did not observe the progressive flattening of the Fat-GFP profile to the WPP
249 wing (Fig. 2 - figure supplement 3A). Instead, the Fat-GFP profile was graded at the WPP stage
250 and flattened somewhat more by the BPP stage (Fig. 2 - figure supplement 3B). We also tested
251 whether Fj regulates the Fat expression pattern by examining Fat-GFP in a *fj* mutant. However,
252 the distribution of Fat-GFP was unchanged in the *fj* mutant (Fig. 2 -figure supplement 3C).
253 Therefore, Ds regulates the dynamics of Fat protein expression.

254

255 **The Ds gradient directly scales with pouch volume**

256 The Ds gradient scales with the size of the wing pouch as measured along the length of
257 the AP axis of symmetry (Fig. 2E). Since the wing pouch can be approximated as an ellipse, the
258 scaling we measured was possibly one related to pouch area. However, the wing pouch is a 3D
259 structure and so Ds gradient scaling might be coupled to wing volume rather than area. To test

260 this idea, we altered the dimensions of the wing pouch without changing its volume. Perlecan is
261 a basement membrane proteoglycan required for extracellular matrix functionality across many
262 tissues (Gubbiotti et al., 2017). Knockdown of perlecan expression by RNAi causes wing disc
263 cells to become thinner and more elongated due to the altered extracellular matrix in the wing
264 disc (Kirkland et al., 2020). We used a Gal4 driver under the control of the *actin5C* promoter
265 (*actin5C-Gal4*) to knock down *trol* gene expression via UAS-RNAi. The *trol* gene encodes
266 perlecan. We measured the dimensions of the wing pouch at the WPP stage and observed that
267 *actin5C>trol*(RNAi) caused a reduction in the area of the wing pouch and an increase in the
268 thickness of the wing pouch (Fig. 3A,B). The overall change in pouch dimensions had no effect
269 on wing pouch volume (Fig. 3C). We then measured the Ds-GFP profile at WPP stage and
270 found *actin5C>trol*(RNAi) had no effect on the gradient (Fig. 3D). Thus, Ds appears to scale
271 with the volume and not the area of the wing pouch. We also examined Fat-GFP to see if its
272 dynamics were altered, and found the gradient flattened normally at the WPP stage (Fig. 3E).
273 Ds gradient might directly scale to wing pouch volume or it might be a consequence of
274 scaling to another feature such as cell number, which correlates with wing volume. To test this
275 possibility, we decreased cell number while keeping total volume constant by over-expressing
276 the cell cycle inhibitor RBF. Using a Gal4 driver under the control of the *engrailed* (*en*) promoter,
277 a *UAS-RBF* transgene was overexpressed in the posterior (P) compartment of the wing disc.
278 Previous work had found such overexpression resulted in half the number of cells in the P
279 compartment but they were two-fold larger in size, such that the P compartment size was
280 unchanged relative to the anterior (A) compartment (Neufeld et al., 1998). We confirmed that
281 *en>RBF* generated fewer and larger P cells, and the ratio of P/A compartment ratio was
282 unchanged (Fig. 3F,G). Nevertheless, the Ds gradient in the P compartment at WPP stage was
283 indistinguishable from wildtype (Fig 3H). The Fat gradient also flattened normally at the WPP
284 stage (Fig. 3I). In summary, the Ds gradient appears to directly scale to wing pouch volume as
285 the pouch grows in size. Fat gradient flattening also appears to be coupled to pouch volume

286 rather than cell number or pouch area. Therefore, the dynamics of these atypical cadherins are
287 coupled to a global physical feature of the wing.
288
289 **Fat and Ds regulate allometric wing growth**

290 We next wanted to understand how Fat and Ds regulate growth of the wing pouch. Prior
291 work had shown that loss-of-function *fat* mutants delay the larva-pupa molt and overgrow the
292 wing disc (Bryant et al., 1988). We applied our quantitative growth analysis pipeline on loss-of-
293 function *fat* mutants. Mutant larvae did not stop growing at 4.5 days AEL as wildtype larvae did,
294 but continued to increase in weight for another day until they entered the non-feeding stage and
295 pupated (Fig. 4A,B). The mutant larval notum and wing pouch grew at a faster rate than normal,
296 and at the larva-pupa molt, the wing pouch continued to grow (Fig. 4C,D and Fig. 4 -figure
297 supplement 1A,B).

298 Loss-of-function *ds* mutants also delayed the larva-pupa molt but only by 12 hours.
299 Mutant larvae continued to gain weight past the wildtype plateau, and they only ceased weight
300 gain at the larva-pupa molt (Fig. 4A,B). The mutant larval notum and wing pouch grew at a rate
301 comparable to those of wildtype, but their growth period was extended (Fig. 4C and Fig. 4 -
302 figure supplement 1A). While the mutant notum ceased to grow prior to the larva-pupa molt, the
303 wing pouch only stopped growing at the BPP stage (Fig. 4D and Fig. 4 - figure supplement 1B).

304 Allometric growth of the *fat* and *ds* mutant wing pouch was significantly different from
305 wildtype (Fig. 4E). In wildtype, there are two linear phases to wing allometric growth (Fig. 1G).
306 Allometric growth of the *ds* and *fat* mutant wing pouches had a first phase that was more
307 extended than normal and a second phase that was less extended than normal (Fig. 4E).
308 Similar trends were observed for allometric growth of the notum in these mutants (Fig. 4 -figure
309 supplement 1C).
310
311 **Autonomous effects of Fat and Ds on wing growth**

312 Fat and Ds proteins are extensively expressed throughout the developing *Drosophila*
313 body, and their loss has clear effects on overall body growth (Mahoney et al., 1991; Clark et al.,
314 1995). Therefore, we wished to know what the wing-autonomous effects of Fat and Ds are on
315 allometric growth. We used the *nubbin-Gal4* (*nub-Gal4*) driver, which is expressed in the wing
316 pouch and distal hinge (Zirin and Mann, 2007), to knock down *fat* and *ds* gene expression via
317 UAS-RNAi (Fig. 5A). The RNAi resulted in near-complete depletion of Fat and Ds proteins in the
318 wing pouch (Fig. 5 - figure supplement 1A-D).
319 As expected, knockdown of either *fat* or *ds* in the wing pouch had no effect on body
320 growth of larvae, and animals reached a normal final weight setpoint (Fig. 5B,C). The third instar
321 stage ended at the same time as for wildtype. Knockdown of both *fat* and *ds* together (*nub>fat*
322 *ds*(RNAi)) in the wing pouch had a slight effect on larval growth but animals reached their
323 normal weight setpoint at the normal time (Fig. 5B,C). Thus, *fat* and *ds* are not required in the
324 wing to limit body growth.
325 Knockdown of *ds* caused the wing pouch to grow at a faster rate than normal. The wing
326 pouch was 28% larger at the WPP stage and continued to grow an additional 14% to the BPP
327 stage (Fig. 5D,E). Knockdown of *fat* had a weak effect; *nub>fat*(RNAi) wings at WPP stage were
328 approximately 11% larger than controls but were no larger at the BPP stage (Fig. 5D,E). The
329 weak effect was not due to incomplete knockdown, since increasing the number of *UAS-*
330 *fat*(RNAi) transgenes did not lead to more overgrowth (data not shown). Knockdown of both *fat*
331 and *ds* together resulted in wing growth that resembled growth of *nub>ds*(RNAi), although the
332 final wing size was slightly larger when both *fat* and *ds* were knocked down (Fig. 5D,E). In
333 contrast, notum growth in *nub>fat*(RNAi)*, nub>ds*(RNAi)*,* and *nub>fat ds*(RNAi) animals was
334 similar to controls, which would be expected if the genes were not required in the wing pouch for
335 notum growth control (Fig. 5 - figure supplement 2). In conclusion, the autonomous effects of *fat*
336 and *ds* on wing growth were less severe than those of whole-body loss of *fat* and *ds*, suggesting
337 there are additional, non-autonomous requirements for Fat/Ds in wing growth.

338 Allometric growth of the wing pouch was also examined (Fig. 5F). Knockdown of *ds*
339 caused the entire allometric relationship to shift such that *nub>ds*(RNAi) wings were
340 consistently bigger for their given body size. A similar trend was observed for *nub>fat ds*(RNAi)
341 wings, although like the *fat* loss-of-function mutant, the first linear phase of allometric growth
342 was extended (Fig. 5F). In summary, it appears that Ds is required to tune down the allometric
343 relationship of the wing to the body. Allometric wing growth appears to have little autonomous
344 need for Fat alone. However, Fat may have some overlapping function with Ds since allometric
345 growth of *nub>fat ds*(RNAi) wings is slightly different from *nub>ds*(RNAi) wings.
346 To further explore the autonomous requirements for Fat and Ds, we used *ap-Gal4* to
347 specifically drive *ds* RNAi in the dorsal (D) compartment of the wing disc (Fig. 5G). This allowed
348 us to measure growth effects by comparing the affected D compartment to the unaffected
349 ventral (V) compartment, serving as an internal control. As expected, RNAi resulted in
350 undetectable Ds protein in the D compartment, though it was detected in the V compartment
351 (Fig. 5 - figure supplement 1E). We measured the final set-point size of each compartment in
352 the wing pouch. Knockdown of *ds* caused the D/V ratio of compartment size to increase by 60%
353 (Fig. 5H). Overall wing pouch size was unaffected by *ap>ds*(RNAi) knockdown (Fig 5I) since
354 there are mechanisms in which the compartments sense overall pouch size, resulting in
355 undergrowth of one compartment when there is overgrowth in the other compartment (Diaz-
356 Benjumea and Cohen, 1993). We also used an *en-Gal4* driver to specifically generate RNAi of
357 *fat* or *ds* in the posterior (P) compartment of the wing disc (Fig. 5L). As expected, RNAi resulted
358 in undetectable Fat and Ds proteins in the P compartment but not the anterior (A) compartment
359 (Fig. 5 - figure supplement 1F,G). After knockdown, the P/A ratio of compartment size was
360 increased by 63% and 23% in *en>ds*(RNAi) and *en>fat*(RNAi) wing pouches, respectively (Fig.
361 5M). This was consistent with wing pouch knockdown of the genes, where *nub>ds*(RNAi) was
362 more severe than *nub>fat*(RNAi) (Fig. 5D,E). *en>fat ds*(RNAi) showed an increase in the P/A
363 ratio by 193%, a synergistic effect greater than the sum of effects from knockdown of each

364 individual gene alone (Fig. 5M). This synergism had not been observed in the *nub-Gal4*
365 knockdown experiments (Fig. 5D,E). Possibly non-autonomous effects of knockdown in the P
366 compartment of the notum are influencing wing pouch growth properties. *en>fat*(RNAi),
367 *en>ds*(RNAi), and *en>fat ds*(RNAi) affected overall wing pouch size to a lesser extent, with
368 respective 10%, 19%, and 32% increases (Fig 5N).
369
370 **Ds and Fat regulate wing pouch size by affecting cell proliferation**
371 To determine whether Ds regulates cell number, cell size or both, we segmented cells in
372 the imaged wing pouch of *ap>ds*(RNAi) WPP animals using E-cadherin tagged with mCherry to
373 outline the apical domains of cells. We used a computational pipeline that segments imaginal
374 disc cells with >99% accuracy (Gallagher et al., 2022). The number of *ds*(RNAi) cells in the D
375 compartment was 42% higher than the wildtype control (Fig. 5J). The average size of *ds*(RNAi)
376 cells in the D compartment, as measured by apical domain area, was unchanged (Fig. 5K).
377 Thus, the enhanced size of *ds*(RNAi) wing pouches is primarily driven by an increase in cell
378 number.
379 Ds might autonomously regulate wing cell number by stimulating apoptosis or by
380 inhibiting cell proliferation. There is little to no apoptosis reported to occur in the third instar
381 larval wing pouch (Milan et al., 1997), which we confirmed by anti-caspase 3 staining (data not
382 shown). To monitor cell proliferation, we developed a method to infer the average cell cycle time
383 from fixed and stained wing discs. Discs were stained with anti-PHH3, which exclusively marks
384 cells in M phase of the cell cycle. During the third instar larval stage, sporadic PHH3-positive
385 cells are uniformly distributed throughout the wing pouch, as expected for uniform asynchronous
386 proliferation (Fig. 1 - figure supplement 4A,B). Using manual and computational segmentation of
387 the images, we identified and counted the number of wing cells in M phase and also counted
388 the total number of wing cells. The ratio of number of M-phase cells to total cells is known as the
389 mitotic index (MI). We found the average time for third instar larval wing pouch cells to transit M

390 phase to be 20.5 min or 0.34 hr (Fig. 6 - figure supplement 1), which is highly similar to previous
391 measurements (Wartlick et al., 2011). Therefore, the average cell cycle time T_{cc} can be inferred
392 as

393 $$T_{cc} = \frac{0.34\ hr}{MI}$$

394 We then estimated the average cell cycle time for the wing pouch at various times during
395 the third instar larval stage. It had been previously reported that there was a progressive
396 lengthening of the cell cycle over developmental time (Fain and Stevens, 1982; Wartlick et al.,
397 2011). Our results corroborated these reports but also expanded upon them, finding that the
398 average cell cycle time linearly scales with wing pouch volume (Fig. 6A). The estimated *scaling*
399 *coefficient* (slope of the linear fit) predicts that the cell cycle length increases 16 hr as wing
400 pouch volume increases by 1 nL.

401 We then estimated T_{cc} for the wing pouch in which *ds* was knocked down by *nub-Gal4*
402 driven RNAi. The *nub*>*ds*(RNAi) cell cycle time linearly scaled with wing pouch volume (Fig.
403 6B). However, the scaling coefficient for *ds*(RNAi) cells was much smaller than wildtype (p = 6.2
404 $\times 10^{-4}$). This meant that cell cycle duration was not lengthening as rapidly as normal and so cell
405 cycle times were consistently shorter. The shorter cell cycle in *nub*>*ds*(RNAi) cells would
406 account for the higher growth rate of the wing pouch size observed for *nub*>*ds*(RNAi) (Fig. 5D).

407 We also examined the scaling relationship between cell cycle time and wing pouch
408 volume when *fat* was knocked down by *nub-Gal4* driven RNAi (Fig. 6C). The scaling coefficient
409 for *nub*>*fat*(RNAi) cells was highly similar to the wildtype control. This is consistent with our
410 observation that wing pouch size in *nub*>*fat*(RNAi) animals was close to normal (Fig. 5D).
411 Finally, we examined the scaling between cell cycle time and wing pouch volume when both *ds*
412 and *fat* were simultaneously knocked down by *nub-Gal4* driven RNAi (Fig. 6D). This resulted in
413 a much smaller scaling coefficient than normal (p = 9.6 $\times 10^{-6}$), which was similar to the *ds*(RNAi)
414 effect on the scaling coefficient (p = 0.089 comparing *ds*(RNAi) to *fat ds*(RNAi) (Fig. 6E).

415 In summary, Fat and Ds regulate a mechanism that couples the duration of the cell cycle
416 to overall wing pouch size. They are not essential for the coupling mechanism itself but rather
417 they tune the mechanism so as to ensure the growth rate of the wing is attenuated relative to
418 the body. This coordinates the relative scaling of the wing to the final body size.
419
420 **The gradients of Fat and Ds protein have little effect on wing pouch growth**
421 Fat and Ds regulate the mechanism by which the cell cycle progressively lengthens as
422 wing size increases, ensuring a proper allometric growth relationship between wing and body.
423 As the wing grows in size, the complementary gradients of Fat and Ds protein across the wing
424 pouch progressively diminish in steepness. These observations suggest a hypothesis that
425 connects the two; namely, wing growth progressively slows because the Fat and Ds gradients
426 become shallower, and growth ultimately ceases when the Fat gradient flattens. To test the
427 hypothesis, we used *nub-Gal4*, which drives graded expression in the larval wing pouch, high in
428 the center of the pouch and low at the margins (Fig. 7A). Using *nub-Gal4* to express *UAS-ds,*
429 we were able to reverse the normal Ds protein gradient (Fig. 7B-D and Fig. 7 - figure
430 supplement 1A). A peak of Ds was centered along the DV axis and skewed towards the anterior
431 along the AP axis. As larvae reached the end of the third instar, the artificial gradient became
432 shallower but was still reversed. Interestingly, the reversed Ds gradient caused a change in the
433 Fat gradient (Fig. 7E). Its peak also became skewed to the anterior and did not normally flatten
434 at the WPP stage. We then measured growth in the *nub>ds* larvae (Fig. 7 - figure supplement
435 1B-E). The growth curve of the larval wing pouch was indistinguishable from wildtype, and wing
436 growth ceased normally at the WPP stage of the larva-pupa molt (Fig. 7 - figure supplement
437 1D,E). This result suggests that the dynamics of graded Ds expression do not control wing
438 growth.
439 The Fat protein profile did not flatten at the WPP stage in *nub>ds* animals, and yet wing
440 growth ended. It suggests that the flattening of the Fat gradient does not trigger growth

441 cessation. To further test this idea, we expressed HA-tagged Fat using the *nub-Gal4* driver
442 without eliminating endogenous Fat (Fig. 7F and Fig. 7 - figure supplement 2A). We monitored
443 both transgenic and endogenous sources of Fat protein, and found both were distributed across
444 the wing pouch in a gradient that was highest in the pouch center (Fig 7G,H). Strikingly, both
445 transgenic and endogenous Fat gradients did not diminish in magnitude as larvae approached
446 the pupa molt. Moreover, the gradients did not flatten at the WPP stage but only did so at the
447 later BPP stage. We then examined the growth properties in *nub>fat-HA* animals. The
448 relationship between the cell cycle time in the *nub>fat-HA* wing pouch and wing pouch size was
449 indistinguishable from wildtype (Fig. 7I). This was consistent with the observation that final wing
450 pouch size in *nub>fat-HA* animals was normal (Fig. 7 - figure supplement 2B). In summary, Fat
451 and Ds gradient dynamics do not appear to play a significant role in wing growth control.
452

453 **Discussion**

454 Growth control of the *Drosophila* wing utilizes numerous mechanisms, ranging from
455 systemic mechanisms involving insulin-like peptides and ecdysone secreted from other tissues,
456 to autonomous mechanisms involving paracrine growth factors (Dpp and Wg), Hippo signaling,
457 and cadherin molecules such as Fat and Ds. Here, we have focused on the macroscopic
458 features of Fat and Ds that function in wing growth control. Fat and Ds attenuate the rate of
459 wing growth so that it properly scales with body growth via a complex allosteric relationship.
460 They do so by tuning the rate at which the cell cycle progressively lengthens in a linear fashion
461 as the wing grows in size. This rate of lengthening is enhanced by the actions of Fat and Ds.
462 It has been long known that the cell cycle in the wing disc slows down, with a cell
463 doubling time of 6 hr during the second instar increasing to 30 hr by the end of third instar (Fain
464 and Stevens, 1982; Bryant and Levinson, 1985; Bittig et al., 2009; Martin et al., 2009; Wartlick
465 et al., 2011). Although this phenomenon is expected to have an impact on the overall rate of
466 wing growth, the phenomenon has not been extensively studied. It was found that lengthening

467 of the G2 phase of the cell cycle is primarily responsible for the longer doubling times (Fain and
468 Stevens, 1982). A more recent study found a link between the cell doubling time and the
469 morphogen Dpp (Wartlick et al., 2011). Dpp is continually synthesized in a stripe of cells at the
470 AP midline of the wing disc and is transported to form a stably graded distribution of protein that
471 is bilaterally symmetric around the midline (Teleman and Cohen, 2000). The Dpp gradient is
472 maintained over days of larval development, during which its relative size adapts to the
473 increasing size of the wing disc. The gradient precisely scales to remain proportional to the size
474 of the growing disc by a mechanism involving the extracellular protein Pentagone and tissue-
475 scale transport of recycled Dpp after endocytosis (Ben-Zvi et al., 2011; Hamaratoglu et al.,
476 2011; Wartlick et al., 2011; Wartlick et al., 2014; Zhu et al., 2020; Romanova-Michaelides et al.,
477 2022). As the gradient scales with the wing, the local concentration of Dpp any wing cell
478 experiences continuously increases over time (Wartlick et al., 2011).

479 The doubling time of wing disc cells was found to strongly correlate with this temporal
480 increase in Dpp concentration, such that an average cell divided when Dpp increased by 40%
481 relative to its level at the beginning of the division cycle (Wartlick et al., 2011). This correlation
482 suggests that cell cycle time is defined by a temporal increase in Dpp signaling, a hypothesis
483 supported by mathematical modeling (Averbukh et al., 2014). The correlation was observed
484 across larval development, indicating that progressive lengthening of the cell cycle may be
485 caused by a slowing rate of increase in local Dpp concentration over time.

486 How then might Fat and Ds tune this relationship? Fat acts through an atypical myosin
487 named Dachs; loss of the *dachs* gene completely suppresses the overgrowth phenotype of *fat*
488 mutants (Cho and Irvine, 2004; Mao et al., 2006). Fat signaling inhibits or destabilizes apico-
489 cortical localization of Dachs protein, consistent with the genetically antagonistic roles played by
490 *fat* and *dachs* (Mao et al., 2006; Brittle et al., 2012). Loss of *dachs* also suppresses
491 overproliferation of wing disc cells when a constitutively-active form of the Dpp receptor protein
492 is expressed (Rogulja et al., 2008). In contrast, loss of *fat* enhances Dpp signaling within wing

493 disc cells (Tyler and Baker, 2007). Therefore, it is possible that local Ds and Fat signaling
494 between cells attenuates their sensitivity to Dpp as a mitogen. It would then require a larger
495 temporal increase in Dpp concentration to trigger cells to divide. This model is consistent with
496 our observation that *fat ds* (RNAi) wing cells do not lengthen their cell cycle as rapidly as
497 normal.

498 Fat acts through Dachs to regulate the Hippo pathway (Pan, 2010). Dachs physically
499 binds to Warts when overexpressed in cells and promotes its destruction. It is thought that Fat
500 signals through Warts to attenuate the nuclear abundance of Yki, thus downregulating
501 transcription of Yki target genes. What target genes might mediate the effects of Fat and Ds on
502 cell cycle dynamics in the wing pouch? Target genes such as *myc* and *cycE* regulate the length
503 of G1 phase (Lee and Orr-Weaver, 2003; Gallant, 2013). However, the length of G2 phase was
504 found to determine the progressive lengthening of the cell cycle in the wing (Fain and Stevens,
505 1982). A more likely transcriptional target of Yki might be *bantam*, which indirectly activates
506 Cdc25, a key regulator of the G2/M transition (Oh and Irvine, 2011; Gerlach et al., 2019).
507 Hence, Fat signaling could attenuate *bantam* expression and Cdc25 activity, thus expanding the
508 length of the G2 phase. This mechanism is particularly attractive since the transcriptional
509 effector of Dpp signaling, Mad, also activates *bantam* transcription (Oh and Irvine, 2011). Yki
510 and Mad proteins directly bind one another and associate with an enhancer in the *bantam* gene.
511 Enhancer activity is weaker if Yki is knocked down but Dpp signaling is still present (Oh and
512 Irvine, 2011). Perhaps Fat and Ds tune the cell cycle time though this common effector gene.

513 An alternative model is that Fat and Ds control the rate at which Dpp levels increase in
514 the wing pouch over time. In this model, cells experience a slower rate in the rise of Dpp levels
515 because of Fat/Ds signaling. Evidence to support the model comes from studies finding that the
516 *dally* and *dally-like* (*dlp*) genes are transcriptionally activated by Yki in the wing pouch (Baena-
517 Lopez et al., 2008). Dally and Dlp are glypicans that contribute to boosting the Dpp morphogen
518 gradient range, perhaps by ensuring retention of Dpp at the cell surface (Stapornwongkul and

519 Vincent, 2021). Fat and Ds signaling appears to diminish *dally* and *dlp* expression, and
520 mutations in *dally* and *dlp* suppress the overgrowth phenotypes of *fat* and *ds* (Baena-Lopez et
521 al., 2008).

522 Ds is required in both signal-sending cells as well as signal-responding cells, suggesting
523 that Ds has both ligand- and receptor-like activities (Casal et al., 2006; Willecke et al., 2008).
524 We find growth dependence on Ds and Fat is consistent with such complex activities.
525 Knockdown of Ds alone stimulates growth while knock down of Fat alone does not. Thus, Ds is
526 not solely acting through Fat to signal cells. Knockdown of both Ds and Fat has a slightly
527 stronger effect on growth stimulation. Thus, Fat and Ds have overlapping functions in signaling
528 cells to limit their growth. Absence of both cadherins results in cells having a cell cycle that
529 lengthens in time at a slower pace than normal.

530 Ds and Fat have unusual properties for a ligand and receptor. Based on experiments
531 with clones expressing Ds at different levels than their neighbors, it was suggested that Fat
532 signaling is regulated by the steepness of a Ds gradient across a field of cells (Rogulja et al.,
533 2008; Willecke et al., 2008). A steep gradient of Ds inactivates Fat signaling, whereas a shallow
534 gradient activates Fat signaling. Indeed, we find the natural Ds expression pattern has a graded
535 distribution with a steep slope in the lateral region of the wing pouch (near the margin) and a
536 shallow slope in the medial region of the pouch (near the center). This is consistent with
537 experiments finding Fat primarily inhibits growth in the medial region, where a shallow
538 distribution of Ds occurs (Schwank et al., 2011). We find that Ds not only regulates Fat activity
539 but also its abundance. Fat is distributed in a gradient that is complementary to the Ds gradient -
540 Fat is most abundant in cells where the Ds gradient is lowest and most shallow. Loss of Ds
541 affects the Fat gradient such that distribution of Fat is uniformly upregulated to peak levels.
542 Likewise, inversion of the Ds gradient has a similar effect on Fat distribution. These results
543 suggest that Fat protein levels might be upregulated when cells sense a shallow gradient of Ds.

544 The graded distribution of Fat protein across the pouch is not stable over time but
545 becomes progressively flatter as the larva-pupa molt is reached. The significance of these
546 dynamics is unclear, but the flattening of the Fat gradient is not a trigger for growth cessation.
547 Since Ds regulates the Fat gradient, perhaps Ds activity is variable over time, leading to these
548 dynamics.
549

550 **Materials and Methods**

551 **Key Resource Table**

Reagent type (species) or resource	Designation	Source or reference	Identifiers	Additional information
Gene (*Drosophila melanogaster*)	*E-cadherin-GFP*	Bloomington *Drosophila* Stock Center	BDSC: 60584 Flybase: FBal0247908	
Gene (*Drosophila melanogaster*)	*E-cadherin-mCherry*	Bloomington *Drosophila* Stock Center	BDSC: 59014 Flybase: FBti0168567	
Gene (*Drosophila melanogaster*)	*sfGFP-sens*	Giri et al., 2020	Flybase: FBal0360102	
Gene (*Drosophila melanogaster*)	$fat^{G\text{-}rv}$	Bloomington *Drosophila* Stock Center	BDSC: 1894 Flybase: FBal0004805	
Gene (*Drosophila melanogaster*)	fat^{8}	Bloomington *Drosophila* Stock Center	BDSC: 44257 Flybase: FBal0004794	
Gene (*Drosophila melanogaster*)	fj^{d1}	Bloomington *Drosophila* Stock Center	BDSC: 6373 Flybase: FBal0049500	
Gene (*Drosophila melanogaster*)	fj^{p1}	Bloomington *Drosophila* Stock Center	BDSC: 44253 Flybase: FBal0049503	
Gene (*Drosophila melanogaster*)	ds^{UAO71}	Bloomington *Drosophila* Stock Center	BDSC: 41784 Flybase: FBal0089339	
Gene (*Drosophila melanogaster*)	ds^{33k}	Bloomington *Drosophila* Stock Center	BDSC: 1580 Flybase: FBal0028155	
Gene (*Drosophila melanogaster*)	*ds-GFP*	Brittle et al., 2012	Flybase: FBal0344517	Gift from Ken Irvine

Gene (*Drosophila melanogaster*)	*fat-GFP*	Hale et al., 2015	Flybase: FBal0385338	Gift from Helen McNeill
Gene (*Drosophila melanogaster*)	*UAS-fat-HA*	Sopko et al., 2009	Flybase: FBal0239166	Gift from H. McNeill
Gene (*Drosophila melanogaster*)	*UAS-ds*	Matakatsu and Blair, 2004	Flybase: FBal0180099	Gift from Ken Irvine
Gene (*Drosophila melanogaster*)	*UAS-bazooka-mCherry*	Bloomington *Drosophila* Stock Center	BDSC: 65844 Flybase: FBti0183177	
Gene (*Drosophila melanogaster*)	*UAS-fat*(RNAi)	Bloomington *Drosophila* Stock Center	BDSC: 34970 Flybase: FBti0144840	
Gene (*Drosophila melanogaster*)	*UAS-ds*(RNAi)	Bloomington *Drosophila* Stock Center	BDSC: 32964 Flybase: FBti0140473	
Gene (*Drosophila melanogaster*)	*UAS-trol*(RNAi)	Bloomington *Drosophila* Stock Center	BDSC: 29440 Flybase: FBti0129068	
Gene (*Drosophila melanogaster*)	*UAS-RBF*	Bloomington *Drosophila* Stock Center	BDSC: 50747 Flybase: FBti0016888	
Gene (*Drosophila melanogaster*)	*ap-Gal4*	Bloomington *Drosophila* Stock Center	BDSC: 3041 Flybase: FBti0002785	
Gene (*Drosophila melanogaster*)	*nub-Gal4*	Bloomington *Drosophila* Stock Center	BDSC: 42699 Flybase: FBal0277528	
Gene (*Drosophila melanogaster*)	*en-Gal4*	Bloomington *Drosophila* Stock Center	BDSC: 30564 Flybase: FBti0003572	
Gene (*Drosophila melanogaster*)	*da-Gal4*	Bloomington *Drosophila* Stock Center	BDSC: 55850 Flybase: FBti0013991	
Gene (*Drosophila melanogaster*)	*actin5c-Gal4*	Bloomington *Drosophila* Stock Center	BDSC: 3954 Flybase: FBti0012292	
Gene (*Drosophila melanogaster*)	*UAS-GFP-NLS*	Bloomington *Drosophila* Stock Center	BDSC: 4776 Flybase: FBti0012493	
Gene (*Drosophila melanogaster*)	*5xQE-dsRed*	Zecca and Struhl, 2007	Flybase: FBal0219107	Gift from Gary Struhl
Antibody	mouse anti-Wg	Developmental Studies Hybridoma Bank	4D4	IF (1:1000)
Antibody	mouse anti-En	Developmental Studies Hybridoma Bank	4D9	IF (1:15)
Antibody	rat anti-E-cadherin	Developmental Studies Hybridoma Bank	Dcad2	IF (1:10)

Antibody	rat anti-Ds			IF (1:1000), Gift from Helen McNeill
Antibody	rat anti-HA	Roche		IF (1:1000)
Antibody	rabbit anti-PHH3	Sigma	H0412	IF (1:400)
Antibody	Goat anti-Rabbit Alexa Fluor 546	Invitrogen	A11035	IF (1:200)
Antibody	Goat anti-Mouse Alexa Fluor 405	Invitrogen	A48255	IF (1:200)
Antibody	Goat anti-Rat Alexa Fluor 647	Invitrogen	A48265	IF (1:200)
Other	18x18 mm number 1.5 coverslip	Zeiss	474030-9000-000	
Other	24x60 mm number 1.5 coverslip	VWR	48393-251	
Chemical compound, drug	Vectashield Plus	Vector Labs	H-1900	
Chemical compound, drug	4′,6-diamidino-2-phenylindole (DAPI)	Life Technologies	D1306	
Chemical compound, drug	Triton X-100	Sigma Aldrich	T9284-500ML	
Chemical compound, drug	Paraformaldehyde (powder)	Polysciences	00380–1	
Software, algorithm	ImSAnE MATLAB software	Heemskerk and Streichan, 2015	https://github.com/idse/imsane	
Software, algorithm	Trained CNN model for pixel classification of epithelial fluorescence confocal data	Gallagher et al., 2022	https://drive.google.com/drive/folders/1I-nRpn1esRzs5t4ztgbNvkBQuTN2vT7L?usp=sharing	
Software, algorithm	MATLAB pipeline to estimate larval volume	This paper	https://github.com/andrewliu321/LarvaSeg	
Software, algorithm	MATLAB pipeline to measure protein fluorescent intensity in the wing pouch	This paper	https://github.com/andrewliu321/ProteinIntensity	

Experimental model and subject details

Animals were raised at 25°C under standard lab conditions on molasses-cornmeal fly food. Only males were analyzed in experiments. For staged collections, 100 adult females were crossed with 50 adult males and allowed to lay eggs for 4 hours (6 pm to 10 pm) in egg-laying

557 cages with yeast paste. First-instar larvae that hatched between 7 and 9 pm the following day
558 were collected, thus synchronizing age to a 2-hour hatching window. Approximately 200 - 300
559 larvae were transferred into a bottle. Third-instar larvae were collected from the bottle every 12
560 hours at 8 am and 8 pm, from 3.5 days after egg laying (AEL) until pupariation (i.e., 5 days for
561 wildtype). We also collected animals at the white-prepupae (WPP) stage and the brown-
562 prepupae (BPP) stage. The BPP stage is 1 hour after the WPP stage, when the pupal case
563 begins to turn brown (Bainbridge and Bownes, 1981).

564 Collected animals were weighed in batches of 5 individuals to account for instrument
565 sensitivity. They were individually photographed using a Nikon SMZ-U dissection scope
566 equipped with a Nikon DS-Fi3 digital camera at 1920 x 1200 resolution with a 8 μm x-y pixel
567 size. Length and width were measured in a custom-built Matlab pipeline as follows. The outline
568 of the body was recorded with manual inputs. The midline was calculated by the Matlab bwskel
569 function and manually corrected. The midline was recorded as the length. At every pixel along
570 the midline, a perpendicular line was computed, and the width recorded. The mean width was
571 then calculated. We approximated the volume of each larva by treating it as a cylinder and using
572 the measured length and average width of the larva for length and diameter, respectively.

573 **Genetics**

574 *fat-GFP* (Hale et al., 2015) and *ds-GFP* (Brittle et al., 2012) are tagged at their ORF carboxy-
575 termini within the respective endogenous genes. This had been done using homologous
576 recombination and pRK2 targeting vectors. The *vg 5xQE-dsRed* transgenic line expresses
577 fluorescent protein specifically in wing pouch cells (Kim et al., 1996; Zecca and Struhl, 2007). To
578 mark proneural cells in the wing pouch, we used *sfGFP-sens* (Giri et al., 2020), which is a N-
579 terminal tag of GFP in the *senseless* (*sens*) gene. To count cell numbers we used either *E-*
580 *cadherin-GFP,* which has GFP fused at the carboxy-terminus of the ORF in the endogenous

581 *shotgun* gene, or *E-cadherin-mCherry*, which has mCherry fused at the endogenous carboxy-
582 terminus (Huang et al., 2009).

583 Loss of function *fat* alleles used were: fat^{8}, with a premature stop codon inserted at
584 S981; and $fat^{G\text{-}rv}$, with a premature stop codon at S2929 (Matakatsu and Blair, 2006). Loss of
585 function *ds* alleles used were: ds^{33k}, derived by X-ray mutagenesis and expected to produce a
586 truncated protein without function; and ds^{UAO71}, derived by EMS mutagenesis and presumed to
587 be amorphic (Clark et al., 1995; Adler et al., 1998). Loss of function *fj* alleles used were: fj^{p1}, in
588 which P{LacW} is inserted into the 5' UTR; and fj^{d1} in which sequences accounting for the N-
589 terminal 100 amino acids are deleted. For all experiments using loss of function mutants, we
590 crossed heterozygous mutant parents to generate trans-heterozygous mutant offspring for
591 study. This minimized the impact of secondary mutations on phenotypes.

592 To measure expression driven by *nub-Gal4* (Bloomington Drosophila Stock Center
593 BDSC # 42699), we used *UAS-GFP-NLS* (BDSC # 4776). To change Ds expression, *fat-GFP*,
594 *nub-Gal4* flies were crossed to *fat-GFP*; *UAS-ds* flies. *UAS-ds* (Matakatsu and Blair, 2004) was
595 a gift from Ken Irvine. To change Fat expression, *fat-GFP*, *nub-Gal4* flies were crossed to *fat-*
596 *GFP*, *UAS-fat-HA* flies. *UAS-fat-HA* expresses Fat with a C-terminal HA tag (Sopko et al.,
597 2009). To test whether Fat expression is transcriptionally regulated, *fat-GFP*; *da-Gal4* flies were
598 crossed to *fat-GFP*, *UAS-fat-HA*; *UAS-Bazooka-mCherry*. *da-Gal4* (BDSC # 55850) and *UAS-*
599 *Bazooka-mCherry* (BDSC # 65844) were used.

600 To knockdown Fat in the wing pouch and distal hinge, *fat-GFP*, *nub-Gal4* flies were
601 crossed to *fat-GFP*; *UAS-fat-RNAi* flies. The RNAi vector is a TRiP Valium 20 (BDSC # 34970).
602 To knockdown Ds in the wing pouch and distal hinge, *fat-GFP*, *nub-Gal4* flies were crossed to
603 *fat-GFP*; *UAS-ds-RNAi* flies. The RNAi vector is a TRiP Valium 20 (BDSC # 32964). To
604 knockdown both genes, *fat-GFP*; *UAS-fat-RNAi*, *UAS-ds-RNAi* flies were crossed to *fat-GFP*,

605 *nub-Gal4* flies. To knockdown Fat specifically in the posterior compartment, *fat-GFP*, *en-Gal4*
606 flies were crossed to *fat-GFP*; *UAS-fat-RNA* flies. *en-Gal4* flies were from BDSC # 30564. To
607 knockdown Ds specifically in the posterior compartment, *ds-GFP*, *en-Gal4* flies were crossed to
608 *ds-GFP*; *UAS-ds-RNAi* flies. To knockdown both genes, *fat-GFP*; *UAS-fat-RNAi*, *UAS-ds-RNAi*
609 were crossed to *fat-GFP*, *en-Gal4* flies. To knockdown Ds specifically in the dorsal
610 compartment, *ds-gfp, ap-Gal4* flies (BDSC # 3041) were crossed to *E-cadherin-mCherry*; *UAS-*
611 *ds-RNAi* flies.

612 To alter cell number, *en-Gal4* flies were crossed to *UAS-RBF* (BDSC # 50747). The
613 crosses also carried either *ds-GFP* or *fat-GFP* so that resulting animals had two copies of each
614 gene. To alter wing disc area and thickness, *actin5c-Gal4* (BDSC # 3954) flies were crossed to
615 *UAS-trol-RNAi* flies. The RNAi line is a TRiP Valium 10 (BDSC # 29440). The crosses also
616 carried either *ds-GFP* or *fat-GFP* so that resulting animals had two copies of each gene.

617 **Immunohistochemistry**

618 Wing discs were fixed in 4% (w/v) paraformaldehyde in PBS at room temperature for 20
619 min and washed three times for 5-10 min each with PBS containing 0.1% (v/v) Triton X-100
620 (PBSTx). The following primary antibodies were used: rat anti-Ds (1:1,000, a gift from Helen
621 McNeill), mouse anti-Wg (1:1000, Developmental Studies Hybridoma Bank DHSB # 4D4),
622 mouse anti-En (1:15, DHSB # 4D9), rat anti-HA (1:1000, Roche), rat anti-E-cadherin (1:10,
623 DHSB # Dcad2), and rabbit anti-PHH3 (1:400, Sigma # H0412). All antibodies were diluted in
624 PBSTx and 5% (v/v) goat serum and incubated overnight at 4°C. After 5 washes in PBSTx,
625 discs were incubated at room temperature for 90 min with the appropriate Alexa-fluor secondary
626 antibodies (Invitrogen #'s A11035, A48255, or A48265) diluted 1:200 in PBSTx and 5% goat
627 serum. After 3 washes in PBSTx, between 5 - 40 wing discs were mounted in 40 µL of
628 Vectashield Plus between a 18x18 mm number 1.5 coverslip (Zeiss # 474030-9000-000) and a

629 24x60 mm number 1.5 coverslip (VWR # 48393-251). Mounting between two coverslips allowed
630 the samples to be imaged from both directions. The volume of mounting media used was critical
631 so that discs were not overly compressed by the coverslips. Compression led to fluorescent
632 signals from the peripodial membrane to be too close in z-space to the disc proper, making it
633 difficult to distinguish the two during image processing.

634 **Single molecule fluorescence in situ hybridization (smFISH)**

635 A set of 45 non-overlapping oligonucleotide probes complementary to the GFP sense sequence
636 were labeled with Alexa 633. The set is described in Bakker et al. (2020). We used the protocol
637 of Bakker et al. (2020) to detect *fat-GFP* and *ds-GFP* mRNAs in wing discs. Discs were
638 counterstained with DAPI to visualize nuclei and mounted in Vectashield.

639 **Live disc imaging**

640 Wing discs were dissected from third instar larvae bearing two copies of *E-cadherin-GFP*.
641 These were cultured ex-vivo in live imaging chambers following the protocol exactly as
642 described in Gallagher et al. (2022). The samples were imaged using an inverted microscope
643 (Leica DMI6000 SD) fitted with a CSU-X1 spinning-disk head (Yokogawa) and a back-thinned
644 EMCCD camera (Photometrics Evolve 512 Delta). Images were captured every 5 minutes with
645 a 40x objective (NA = 1.3) at 512 x 512 resolution with a 0.32 μm x-y pixel size.

646 **Image acquisition of fixed samples**

647 All experiments with fixed tissues were imaged using a Leica SP8 confocal microscope.
648 Whole wing discs were imaged using a 10x air objective (NA = 0.4) and 0.75x internal zoom at
649 1024 x 1024 resolution, with a 1.52 μm x-y pixel size. Wing pouches were imaged using a 63x
650 oil objective (NA = 1.4) and 0.75x internal zoom at 1024 x 1024 resolution, with a 0.24 μm x-y
651 pixel size and 0.35 μm z separation. Scans were collected bidirectionally at 600 MHz and were

652 3x line averaged in the following channels to detect: anti-PHH3 (blue), Fat-GFP and Ds-GFP
653 (green), anti-Wg and anti-En (red), and anti-HA or anti-Ds or anti-E-cadherin (far red). Wing
654 discs of different genotypes and similar age were mounted on the same microscope slide and
655 imaged in the same session for consistency in data quality.

656 **Image processing**

657 Raw images were processed using a custom-built Matlab pipeline with no prior
658 preprocessing. The pipeline consists of several modules: 1) surface detection, 2) wing disc,
659 pouch, and midline segmentation, 3) volume measurement, 4) fluorescence intensity
660 measurement, 5) cell segmentation, 6) mitotic index measurement.

661 **1) Surface detection.** Fat-GFP and Ds-GFP proteins localize to the apical region of cells in the
662 wing disc proper. These proteins are also localized in cells of the peripodial membrane, which is
663 positioned near the apical surface of the disc proper. In order to get a 2D projection of the signal
664 in the wing disc proper excluding the peripodial membrane signal, we used an open-source
665 software package called ImSAnE – Image Surface Analysis Environment (Heemskerk and
666 Streichan, 2015). The detailed parameters we used have been previously described (Gallagher
667 et al., 2022). Briefly, we used the MIPDetector module to find the brightest z-position of every xy
668 pixel followed by tpsFitter to fit a single layer surface through these identified z-positions. Using
669 the onionOpts function in ImSAnE, we output a 9-layer z-stack, 4 layers above and below the
670 computed surface that capture the entire signal from the wing disc proper. However, this
671 operation still sometimes includes fluorescence signals from the peripodial membrane.
672 Therefore, we manually masked the residual peripodial signal using FIJI 1.53t. The resulting z-
673 stack was sum-projected to form a 2D surface projection of the wing disc proper.

674 **2) Wing disc, pouch, and midline segmentation.** Wing discs were counterstained for both Wg
675 and En proteins, which mark the wing pouch dorsal-ventral (DV) midline and anterior-posterior

676 (AP) midline, respectively. Although both Wg and En proteins were stained with the same Alexa
677 546 fluorescent antibody, the two signals were readily distinguished by their distinct separation
678 in z space. Wg is apically localized in cells of the disc proper and En is nuclear localized more
679 basally in the disc proper. Moreover, the Wg signal was far stronger than En, allowing for
680 detection of its stripe in the posterior compartment even with a max projection.

681 We built a semi-automated Matlab script that computationally segments the wing disc
682 into discrete objects. i) *Wing disc segmentation*. Endogenous Fat-GFP or Ds-GFP signal was
683 used to segment the wing disc from surrounding media. ii) *Wing pouch segmentation.* The 3D
684 morphology of the wing disc creates narrow and deep tissue folds that surround the wing pouch
685 (Fig. 1 - figure supplement 2A). Using these morphological landmarks that were visualized by
686 the Fat-GFP or Ds-GFP signals, the Matlab script recorded user-derived mouse-clicks that
687 defined the wing pouch boundary. This method was validated to be 95.5% accurate when
688 compared to a wing pouch boundary that was defined by the expression boundary of a reporter
689 for the *vestigial* quadrant enhancer, *5x-QE-DsRed* (Fig. 1 - figure supplement 2B,C). iii) *DV*
690 *midline segmentation.* The Wg signal was used to segment the DV midline running through the
691 segmented wing pouch. Since the Wg and En signals are distinguishable in z space, the upper
692 third of the z-stack was max projected to segment Wg. An adaptive threshold of 0.6 was used to
693 binarize the image into Wg-positive pixels. The binarized and raw images were used to inform
694 manual input of the DV midline. iv) *AP midine segmentation.* The En signal was used to
695 segment the AP midline running through the segmented wing pouch. The lower two-thirds of the
696 z-stack was max projected and binarized in En+ pixels. The binarized and raw images were
697 used to inform manual input of the AP midline.

698 **3) Volume measurement.** Areas of each of the segmented objects were calculated by
699 summing the number of pixels in each object and multiplying by the pixel dimensions in xy
700 physical space. Notum-hinge area was calculated by subtracting the segmented pouch area

701 from total segmented wing disc area. The thickness of the wing pouch was measured at the
702 intersection of the AP and DV midlines using the orthogonal views tool in FIJI. The first layer is
703 defined by the initial signal of Fat-GFP or Ds-GFP at this xy position. The last layer is defined by
704 the first appearance of background signal in the composite image. Thickness of the object was
705 calculated by multiplying the sum of z-slices by the z-separation. To calculate the volume of
706 segmented objects, we multiplied the thickness of the object (in μm) by the object's surface area
707 (in μm^2). Conversion from μm^3 to nL units was performed.

708 **4) Fluorescence intensity measurement of Fat-GFP and Ds-GFP.** Fluorescence intensity
709 values were averaged across a vector of 50 pixels length that was orthogonal to the segmented
710 boundary of interest and having 25 pixels residing on each side of the segmented line. These
711 values were then averaged in a sliding window of 100 pixels length that moved along the
712 segmented boundary of interest. Physical distance along the boundaries were measured using
713 ImSAnE function Proper_Dist to account for the curvature of the segmented objects. The
714 intersection of the segmented DV and AP midlines was defined as the center (0,0 μm) of the
715 wing pouch, with the anterior/dorsal annotated in units of negative μm and the posterior/ventral
716 annotated in units of positive μm. A minimum of three wing discs of the same age and genotype
717 were aligned by their (0,0) centers and their fluorescent measurements were averaged along
718 the AP and DV midlines.

719 Older third instar, WPP, and BPP wing discs begin to evert such that the ventral
720 compartment is partially folded underneath the dorsal compartment. However, the ventral
721 compartment can still be accurately segmented to measure area and thickness even under
722 these conditions. For GFP measurements, the folded specimen resulted in dimmer fluorescent
723 signals from the compartment farthest from the objective due to tissue thickness and light
724 scattering. Thus, measurements were limited to the compartment closest to the objective.

725 **5) Cell boundary segmentation.** To count cell numbers and cell sizes in the wing pouch, we
726 analyzed wing discs imaged from *E-cadherin-GFP* or *E-cadherin-mCherry* larvae. We used a
727 machine learning pixel-classification model based on a convolutional neural net to segment cell
728 boundaries in the surface projections. This model was trained on a broad range of image data
729 derived from Cadherin-GFP labeled *Drosophila* imaginal discs (Gallagher et al., 2022). The
730 model is > 99.5% accurate at segmenting cells when compared to ground truth. Cell size
731 (surface area) and number were computed for specific compartments in the wing pouch.

732 **6) Mitotic index measurement.** Phospho-histone H3 (PHH3) has been used to estimate mitotic
733 index previously (Wartlick et al., 2011). Wing discs were immunostained for PHH3, which labels
734 nuclei undergoing mitosis. These nuclei were manually recorded by user-defined mouse clicks
735 at or near the center of each nucleus. Their Euclidean distances relative to the segmented AP
736 and DV midlines were calculated as was the number of PHH3+ cells. To estimate the total cell
737 number in a wing pouch, we used E-cadherin to computationally segment cells as described
738 above. Each imaged wing pouch had a subset of cell boundaries segmented in a subdomain of
739 the pouch. This was then used to calculate cell density: number of segmented cells divided by
740 subdomain area. The density value was multiplied by total wing pouch area to estimate the total
741 number of wing pouch cells for that sample. We then derived an averaged conversion factor to
742 apply to each volume measurement in order to estimate total cell number. This was done by
743 plotting the estimated total cell number versus wing pouch volume for all discs of a given
744 genotype. Linear regression of the data produced an equation to convert pouch volume to cell
745 number (Table 1).

746 **Table 1 Summary statistics of linear regressions**

	Total Cell Number = $\beta_0 + \beta_1$Pouch Volume			
Genotype	β_0	β_1	R^2	*p*
nub-Gal4	352.0 ±187.7	7261.3 ± 355.2	0.95	8.43E-16

nub>ds(RNAi)	653.9 ± 191.0	4533.5 ± 221.5	0.95	8.19E-16
nub>fat(RNAi)	1060.1 ±423.6	7219.3 ± 686.0	0.87	1.34E-08
nub>ds fat(RNAi)	1890.1 ± 648.3	5673.6 ± 555.2	0.82	5.07E-10
nub>fat-HA	2321.5 ± 324.4	5212.9 ± 516.4	0.80	2.65E-10

The number of PHH3+ cells in a wing pouch was divided by the estimated cell number in that wing pouch to obtain the mitotic index, the fraction of cells in M phase at the time of fixation. Average M phase time, measured by live-imaging, was divided by the mitotic index to obtain the average cell cycle time.

Statistical analysis

Statistical tests included two-tailed Student's t-tests to compare between genotypes. We conducted linear regression modeling to fit pouch volume as an independent variable and cell cycle time as a dependent variable. To statistically test for differences between genotypes, we used a multiple linear regression model:

$$T_{cc} = \beta_0 + (\beta_1 \; x \; Volume) + (\beta_2 \; x \; Genotype) + (\beta_3 \; x \; Volume \; x \; Genotype)$$

Genotype was entered into the model as a covariate to test for differences in intercepts of the fits. Interaction of volume x genotype was entered to test for differences in slope of the fits. Linear regression models were plotted with 95% confidence intervals.

Acknowledgements

Fly stocks from Ken Irvine, Helen McNeill, Gary Struhl, and the Bloomington Drosophila Stock Center are gratefully appreciated. Antibodies were gifts from Helen McNeill and purchases from the Developmental Studies Hybridoma Bank. We thank Hamdi Kucukengin for help in processing some of the images. We thank Kevin Gallagher for his advice on building the Matlab

767 pipelines. We thank Jessica Hornick and the Biological Imaging Facility at Northwestern.

768 Financial support was provided from the NIH (GM118144), NSF (1764421), and Simons

769 Foundation (597491).

770

771 **References**

772 Adler, PN, Charlton, J, Liu, J, 1998. Mutations in the cadherin superfamily member gene
773 *dachsous* cause a tissue polarity phenotype by altering Frizzled signaling. Development 125,
774 959-968.

775 Averbukh, I, Ben-Zvi, D, Mishra, S, Barkai, N, 2014. Scaling morphogen gradients during tissue
776 growth by a cell division rule. Development 141, 2150-2156.

777 Baena-Lopez, LA, Nojima, H, Vincent, JP, 2012. Integration of morphogen signalling within the
778 growth regulatory network. Curr Opin Cell Biol 24, 166-172.

779 Baena-Lopez, LA, Rodriguez, I, Baonza, A, 2008. The tumor suppressor genes *dachsous* and
780 *fat* modulate different signalling pathways by regulating *dally* and *dally-like*. Proc Natl Acad Sci
781 U S A 105, 9645-9650.

782 Bainbridge, SP, Bownes, M, 1981. Staging the metamorphosis of *Drosophila melanogaster*. J
783 Embryol Exp Morphol 66, 57-80.

784 Bakker, R, Mani, M, Carthew, RW, 2020. The Wg and Dpp morphogens regulate gene
785 expression by modulating the frequency of transcriptional bursts. Elife 9:e56076.

786 Ben-Zvi, D, Pyrowolakis, G, Barkai, N, Shilo, BZ, 2011. Expansion-repression mechanism for
787 scaling the Dpp activation gradient in *Drosophila* wing imaginal discs. Curr Biol 21, 1391-1396.

788 Bittig, T, Wartlick, O, Gonzalez-Gaitan, M, Julicher, F, 2009. Quantification of growth
789 asymmetries in developing epithelia. Eur Phys J E Soft Matter 30, 93-99.

790 Boggiano, JC, Fehon, RG, 2012. Growth control by committee: intercellular junctions, cell
791 polarity, and the cytoskeleton regulate Hippo signaling. Dev Cell 22, 695-702.

792 Brittle, A, Thomas, C, Strutt, D, 2012. Planar polarity specification through asymmetric
793 subcellular localization of Fat and Dachsous. Curr Biol 22, 907-914.

794 Bryant, PJ, Huettner, B, Held, LI, Jr., Ryerse, J, Szidonya, J, 1988. Mutations at the *fat* locus
795 interfere with cell proliferation control and epithelial morphogenesis in *Drosophila*. Dev Biol 129,
796 541-554.

797 Bryant, PJ, Levinson, P, 1985. Intrinsic growth control in the imaginal primordia of *Drosophila*,
798 and the autonomous action of a lethal mutation causing overgrowth. Dev Biol 107, 355-363.

799 Casal, J, Lawrence, PA, Struhl, G, 2006. Two separate molecular systems, Dachsous/Fat and
800 Starry night/Frizzled, act independently to confer planar cell polarity. Development 133, 4561-
801 4572.

802 Cho, E, Feng, Y, Rauskolb, C, Maitra, S, Fehon, R, Irvine, KD, 2006. Delineation of a Fat tumor
803 suppressor pathway. Nat Genet 38, 1142-1150.

804 Cho, E, Irvine, KD, 2004. Action of *fat, four-jointed, dachsous* and *dachs* in distal-to-proximal
805 wing signaling. Development 131, 4489-4500.

806 Clark, HF, Brentrup, D, Schneitz, K, Bieber, A, Goodman, C, Noll, M, 1995. *Dachsous* encodes a
807 member of the cadherin superfamily that controls imaginal disc morphogenesis in *Drosophila*.
808 Genes Dev 9, 1530-1542.

809 Colombani, J, Bianchini, L, Layalle, S, Pondeville, E, Dauphin-Villemant, C, Antoniewski, C,
810 Carre, C, Noselli, S, Leopold, P, 2005. Antagonistic actions of ecdysone and insulins determine
811 final size in *Drosophila*. Science 310, 667-670.

812 Conlon, I, Raff, M, 1999. Size control in animal development. Cell 96, 235-244.

813 Diaz-Benjumea, FJ, Cohen, SM, 1993. Interaction between dorsal and ventral cells in the
814 imaginal disc directs wing development in *Drosophila*. Cell 75, 741-752.

815 Fain, MJ, Stevens, B, 1982. Alterations in the cell cycle of *Drosophila* imaginal disc cells
816 precede metamorphosis. Dev Biol 92, 247-258.

817 Gallagher, KD, Mani, M, Carthew, RW, 2022. Emergence of a geometric pattern of cell fates
818 from tissue-scale mechanics in the *Drosophila* eye. Elife 11:e77309.

819 Gallant, P, 2013. Myc function in *Drosophila*. Cold Spring Harb Perspect Med 3, a014324.

820 Garoia, F, Guerra, D, Pezzoli, MC, Lopez-Varea, A, Cavicchi, S, Garcia-Bellido, A, 2000. Cell
821 behaviour of *Drosophila fat* cadherin mutations in wing development. Mech Dev 94, 95-109.

822 Gerlach, SU, Sander, M, Song, S, Herranz, H, 2019. The miRNA bantam regulates growth and
823 tumorigenesis by repressing the cell cycle regulator *tribbles*. Life Sci Alliance 2 (4) e201900381.

824 Gilbert, MK, Tan, YY, Hart, CM, 2006. The *Drosophila* boundary element-associated factors
825 BEAF-32A and BEAF-32B affect chromatin structure. Genetics 173, 1365-1375.

826 Giri, R, Papadopoulos, DK, Posadas, DM, Potluri, HK, Tomancak, P, Mani, M, Carthew, RW,
827 2020. Ordered patterning of the sensory system is susceptible to stochastic features of gene
828 expression. Elife 9.

829 Gubbiotti, MA, Neill, T, Iozzo, RV, 2017. A current view of perlecan in physiology and pathology:
830 a mosaic of functions. Matrix Biol 57-58, 285-298.

831 Hale, R, Brittle, AL, Fisher, KH, Monk, NA, Strutt, D, 2015. Cellular interpretation of the long-
832 range gradient of Four-jointed activity in the *Drosophila* wing. Elife **4**:e05789.

833 Hamaratoglu, F, de Lachapelle, AM, Pyrowolakis, G, Bergmann, S, Affolter, M, 2011. Dpp
834 signaling activity requires Pentagone to scale with tissue size in the growing *Drosophila* wing
835 imaginal disc. PLoS Biol 9, e1001182.

836 Heemskerk, I, Streichan, SJ, 2015. Tissue cartography: compressing bio-image data by
837 dimensional reduction. Nat Methods 12, 1139-1142.

838 Huang, J, Zhou, W, Dong, W, Watson, AM, Hong, Y, 2009. Directed, efficient, and versatile
839 modifications of the *Drosophila* genome by genomic engineering. Proc Natl Acad Sci U S A 106,
840 8284-8289.

841 Huxley, JS, Teissier, G, 1936. Terminology of relative growth. Nature 137, 780-781.

842 Ishikawa, HO, Takeuchi, H, Haltiwanger, RS, Irvine, KD, 2008. Four-jointed is a Golgi kinase
843 that phosphorylates a subset of cadherin domains. Science 321, 401-404.

844 Kim, J, Sebring, A, Esch, JJ, Kraus, ME, Vorwerk, K, Magee, J, Carroll, SB, 1996. Integration of
845 positional signals and regulation of wing formation and identity by *Drosophila vestigial* gene.
846 Nature 382, 133-138.

847 Kirkland, NJ, Yuen, AC, Tozluoglu, M, Hui, N, Paluch, EK, Mao, Y, 2020. Tissue mechanics
848 regulate mitotic nuclear dynamics during epithelial development. Curr Biol 30, 2419-2432
849 e2414.

850 Lee, LA, Orr-Weaver, TL, 2003. Regulation of cell cycles in *Drosophila* development: intrinsic
851 and extrinsic cues. Annu Rev Genet 37, 545-578.

852 Leevers, SJ, McNeill, H, 2005. Controlling the size of organs and organisms. Curr Opin Cell Biol
853 17, 604-609.

854 Legoff, L, Rouault, H, Lecuit, T, 2013. A global pattern of mechanical stress polarizes cell
855 divisions and cell shape in the growing *Drosophila* wing disc. Development 140, 4051-4059.

856 Ma, D, Yang, CH, McNeill, H, Simon, MA, Axelrod, JD, 2003. Fidelity in planar cell polarity
857 signalling. Nature 421, 543-547.

858 Mahoney, PA, Weber, U, Onofrechuk, P, Biessmann, H, Bryant, PJ, Goodman, CS, 1991. The
859 *fat* tumor suppressor gene in *Drosophila* encodes a novel member of the cadherin gene
860 superfamily. Cell 67, 853-868.

861 Mao, Y, Kucuk, B, Irvine, KD, 2009. *Drosophila* lowfat, a novel modulator of Fat signaling.
862 Development 136, 3223-3233.

863 Mao, Y, Rauskolb, C, Cho, E, Hu, WL, Hayter, H, Minihan, G, Katz, FN, Irvine, KD, 2006. Dachs:
864 an unconventional myosin that functions downstream of Fat to regulate growth, affinity and gene
865 expression in *Drosophila*. Development 133, 2539-2551.

866 Martin, FA, Herrera, SC, Morata, G, 2009. Cell competition, growth and size control in the
867 *Drosophila* wing imaginal disc. Development 136, 3747-3756.

868 Matakatsu, H, Blair, SS, 2004. Interactions between Fat and Dachsous and the regulation of
869 planar cell polarity in the *Drosophila* wing. Development 131, 3785-3794.

870 Matakatsu, H, Blair, SS, 2006. Separating the adhesive and signaling functions of the Fat and
871 Dachsous protocadherins. Development 133, 2315-2324.

872 Milan, M, Campuzano, S, Garcia-Bellido, A, 1997. Developmental parameters of cell death in
873 the wing disc of *Drosophila*. Proc Natl Acad Sci U S A 94, 5691-5696.

874 Neto-Silva, RM, Wells, BS, Johnston, LA, 2009. Mechanisms of growth and homeostasis in the
875 *Drosophila* wing. Annu Rev Cell Dev Biol 25, 197-220.

876 Neufeld, TP, de la Cruz, AF, Johnston, LA, Edgar, BA, 1998. Coordination of growth and cell
877 division in the *Drosophila* wing. Cell 93, 1183-1193.

878 Nijhout, HF, Callier, V, 2015. Developmental mechanisms of body size and wing-body scaling in
879 insects. Annu Rev Entomol 60, 141-156.

880 Oh, H, Irvine, KD, 2011. Cooperative regulation of growth by Yorkie and Mad through *bantam*.
881 Dev Cell 20, 109-122.

882 Pan, D, 2010. The Hippo signaling pathway in development and cancer. Dev Cell 19, 491-505.

883 Pan, Y, Heemskerk, I, Ibar, C, Shraiman, BI, Irvine, KD, 2016. Differential growth triggers
884 mechanical feedback that elevates Hippo signaling. Proc Natl Acad Sci U S A 113, E6974-
885 E6983.

886 Penzo-Mendez, AI, Stanger, BZ, 2015. Organ-Size Regulation in Mammals. Cold Spring Harb
887 Perspect Biol 7, a019240.

888 Rauskolb, C, Sun, S, Sun, G, Pan, Y, Irvine, KD, 2014. Cytoskeletal tension inhibits Hippo
889 signaling through an Ajuba-Warts complex. Cell 158, 143-156.

890 Rogulja, D, Rauskolb, C, Irvine, KD, 2008. Morphogen control of wing growth through the Fat
891 signaling pathway. Dev Cell 15, 309-321.

892 Romanova-Michaelides, M, Hadjivasiliou, Z, Aguilar-Hidalgo, D, Basagiannis, D, Seum, C,
893 Dubois, M, Julicher, F, Gonzalez-Gaitan, M, 2022. Morphogen gradient scaling by recycling of
894 intracellular Dpp. Nature 602, 287-293.

895 Rulifson, EJ, Kim, SK, Nusse, R, 2002. Ablation of insulin-producing neurons in flies: growth and
896 diabetic phenotypes. Science 296, 1118-1120.

897 Schwank, G, Tauriello, G, Yagi, R, Kranz, E, Koumoutsakos, P, Basler, K, 2011. Antagonistic
898 growth regulation by Dpp and Fat drives uniform cell proliferation. Dev Cell 20, 123-130.

899 Slaidina, M, Delanoue, R, Gronke, S, Partridge, L, Leopold, P, 2009. A *Drosophila* insulin-like
900 peptide promotes growth during nonfeeding states. Dev Cell 17, 874-884.

901 Sopko, R, Silva, E, Clayton, L, Gardano, L, Barrios-Rodiles, M, Wrana, J, Varelas, X,
902 Arbouzova, NI, Shaw, S, Saburi, S, Matakatsu, H, Blair, S, McNeill, H, 2009. Phosphorylation of

903 the tumor suppressor Fat is regulated by its ligand Dachsous and the kinase Discs Overgrown.
904 Curr Biol 19, 1112-1117.

905 Stapornwongkul, KS, Vincent, JP, 2021. Generation of extracellular morphogen gradients: the
906 case for diffusion. Nat Rev Genet 22, 393-411.

907 Strutt, H, Strutt, D, 2002. Nonautonomous planar polarity patterning in *Drosophila*: Dishevelled-
908 independent functions of Frizzled. Dev Cell 3, 851-863.

909 Tanoue, T, Takeichi, M, 2005. New insights into Fat cadherins. J Cell Sci 118, 2347-2353.

910 Teleman, AA, Cohen, SM, 2000. Dpp gradient formation in the *Drosophila* wing imaginal disc.
911 Cell 103, 971-980.

912 Tyler, DM, Baker, NE, 2007. Expanded and Fat regulate growth and differentiation in the
913 *Drosophila* eye through multiple signaling pathways. Dev Biol 305, 187-201.

914 Vrabioiu, AM, Struhl, G, 2015. Fat/Dachsous signaling promotes *Drosophila* wing growth by
915 regulating the conformational state of the NDR kinase Warts. Dev Cell 35, 737-749.

916 Wartlick, O, Julicher, F, Gonzalez-Gaitan, M, 2014. Growth control by a moving morphogen
917 gradient during *Drosophila* eye development. Development 141, 1884-1893.

918 Wartlick, O, Mumcu, P, Kicheva, A, Bittig, T, Seum, C, Julicher, F, Gonzalez-Gaitan, M, 2011.
919 Dynamics of Dpp signaling and proliferation control. Science 331, 1154-1159.

920 Willecke, M, Hamaratoglu, F, Sansores-Garcia, L, Tao, C, Halder, G, 2008. Boundaries of
921 Dachsous Cadherin activity modulate the Hippo signaling pathway to induce cell proliferation.
922 Proc Natl Acad Sci U S A 105, 14897-14902.

923 Williams, CM, 1980. Growth in Insects., in: Locke, M., Smith, D.S. (Eds.), Insect Biology in the
924 Future. Academic Press, New York, pp. 369-383.

925 Zecca, M, Struhl, G, 2007. Recruitment of cells into the *Drosophila* wing primordium by a feed-
926 forward circuit of vestigial autoregulation. Development 134, 3001-3010.

927 Zhang, Y, Wang, X, Matakatsu, H, Fehon, R, Blair, SS, 2016. The novel SH3 domain protein
928 Dlish/CG10933 mediates Fat signaling in *Drosophila* by binding and regulating Dachs. Elife 5.

929 Zhu, Y, Qiu, Y, Chen, W, Nie, Q, Lander, AD, 2020. Scaling a Dpp morphogen gradient through
930 feedback control of receptors and co-receptors. Dev Cell 53, 724-739 e714.

931 Zirin, JD, Mann, RS, 2007. Nubbin and Teashirt mark barriers to clonal growth along the
932 proximal-distal axis of the *Drosophila* wing. Dev Biol 304, 745-758.

933

934 **Figure Legends**

935

936 **Figure 1. Allometric growth of the wing pouch in *Drosophila*.**

(A) Schematic depicting relative size of the wing imaginal discs inside a larva starting from 3 days after egg laying (AEL). The wing pouch (blue) begins everting during larva-pupa molt and eventually becomes the adult wing blade. The notum and hinge (red) surrounding the wing pouch becomes the wing hinge and notum of the adult.

(B) Wet-weight of third instar larvae as a function of age measured every 12 hours. Lines connect average weight measurements, and the shaded region denotes the standard error of the mean.

(C) At 5 days AEL, the larva-pupa molt begins. Wet-weight of wildtype animals at early pupariation stages. Lines connect average weight measurements, and the shaded region denotes the standard error of the mean.

(D) Volume of the wing pouch as a function of age. Lines connect average volume measurements and the shaded region denotes the standard error of the mean.

(E) Volume of wing pouch at early pupariation stages. Lines connect average volume measurements and the shaded region denotes the standard error of the mean.

(F) Schematic depicting isometric growth (green arrow) where growth rates of the organ (wing) and the body are the same, positive allometric growth (orange arrow) where the organ is growing faster than the body, and negative allometric growth (magenta arrow) where the organ is growing slower than the body.

(G) Allometric growth relationship of the wing pouch versus body weight. Dashed line depicts the trajectory for an isometric growth curve. Error bars denote standard error of the mean.

Figure 1 - figure supplement 1. Measured volume of individuals correlates with measured weight throughout the third instar larval and WPP stages. Since the weight of 1 μL water is 1 mg, the wet weight predicted by volume measurements is close to the measured weight. The strong correlation is independent of age and genotype of measured individuals. Genotypes listed are described later in the Results.

Figure 1 - figure supplement 2. Validation of method in defining the wing pouch boundary.

(A) Confocal image of E-cadherin-GFP in a wing disc, which displays folds in the epithelium as morphological landmarks that define the wing pouch. In magenta is the marked wing pouch boundary.

(B) Confocal image of wing disc expression of the *vestigial* gene reporter *5x-QE-dsRed*, which is specifically expressed in the wing pouch. In magenta is the marked wing pouch boundary.

(C) Comparison of wing pouch area measured in third instar larval wing discs using the two methods. Dotted line shows outcome if both methods were in perfect agreement (slope = 1.0000). Linear regression of the measurement data shows the two methods are in strong agreement (slope = 0.9554).

Figure 1 - figure supplement 3. Allometric growth of the notum-hinge in *Drosophila*.

(A) Area of the larval notum-hinge as a function of age. Lines connect average area measurements, and the shaded region denotes the standard error of the mean.

(B) Area of the notum-hinge at early pupariation stages. Lines connect average area measurements, and the shaded region denotes the standard error of the mean.

(C) Allometric growth relationship of the notum-hinge versus body weight. Dashed line depicts the trajectory for an isometric growth curve. Error bars denote standard error of the mean.

Figure 1 - figure supplement 4. Pattern of cell proliferation in the wing pouch as it ages.

(A) Confocal image of a 4-day old larval wing pouch stained with anti-En and anti-Wg on the left and anti-PHH3 on the right. Wg and En label the AP and DV axes, respectively. The pouch boundary is highlighted with a magenta dashed line while the AP axis is illustrated with cyan dashed line. Scale bar is 50 micrometers.

(B) Centroid positions of PHH3-positive nuclei in the 4-day old larval wing pouch are plotted to show the distribution of cell divisions in the wing pouch. Three wing replicates are shown in different colors. Magenta dashed line illustrates a typical wing pouch.

(C) Confocal image of a WPP wing pouch stained with anti-En and anti-Wg on the left and anti-PHH3 on the right. The pouch boundary is highlighted with a magenta dashed line while the AP axis is illustrated with cyan dashed line. Scale bar is 50 micrometers.

(D) Centroid positions of PHH3-positive nuclei in the WPP wing pouch are plotted to show the distribution of cell divisions in the wing pouch. Three wing replicates are shown in different colors. Magenta dashed line illustrates a typical wing pouch. Note the concentration of dividing cells along the AP axis of symmetry, where sensory organ precursor cells are dividing.

(E) Confocal images of a wing pouch from a WPP stage animal stained for anti-PHH3 (left), sfGFP-Senseless (Sens) (center), and the merge (right). Sens is expressed in cells fated to become sensory organ precursors, each of which undergo two rounds of cell division to form a sensory bristle. At the WPP stage, the only cells actively dividing are those with high Sens expression. Scale bar is 50 micrometers.

Figure 2. Dynamics of Ds and Fat protein distributions across the wing pouch.

(A) Schematic representation of E-cadherin, Fat and Ds protein structures, which are endogenously tagged with GFP at the C-terminus. Adapted from Tanoue and Takeichi, 2005.

(B) Schematic of the wing disc depicting the anterior-posterior (AP, blue) and dorsal-ventral (DV, red) axes of symmetry.

(C) Moving line average of Ds-GFP fluorescence as a function of position along the AP axis. Shown are profiles from wing pouches of different ages, as indicated. Shaded regions for each profile represent the standard error of the mean.

(D) Moving line average of Ds-GFP fluorescence as a function of position along the DV axis. Shown are profiles from wing pouches of different ages, as indicated. Shaded regions for each profile represent the standard error of the mean. In the WPP, the pouch begins everting and only a portion of the ventral compartment is visible.

1022 (E) Moving line average of Ds-GFP fluorescence as a function of position along the AP axis
1023 normalized to the total distance of the axis. Shown are profiles from wing pouches of
1024 different ages, each normalized independently.

1025 (F) Moving line average of Ds-GFP fluorescence as a function of position along the DV axis
1026 normalized to the total distance of the axis. Shown are profiles from wing pouches of
1027 different ages, each normalized independently.

1028 (G) Moving line average of Fat-GFP fluorescence as a function of position along the AP axis.
1029 Shown are profiles from wing pouches of different ages, as indicated at right. Shaded
1030 regions for each profile represent the standard error of the mean.

1031 (H) Moving line average of Fat-GFP fluorescence as a function of position along the DV
1032 axis. Shown are profiles from wing pouches of different ages, as indicated at right.
1033 Shaded regions for each profile represent the standard error of the mean.

1034 (I) Moving line average of Fat-GFP fluorescence as a function of position along the AP axis
1035 normalized to the total distance of the axis. Shown are profiles from wing pouches of
1036 different ages, each normalized independently.

1037 (J) Moving line average of Fat-GFP fluorescence as a function of position along the DV axis
1038 normalized to the total distance of the axis. Shown are profiles from wing pouches of
1039 different ages, each normalized independently.

1040 (K) Schematic of the *da-Gal4* driver, active everywhere in the wing disc, expressing *UAS-fat-*
1041 *HA* and *UAS-bazooka-mCherry*.

1042 (L) Moving line averages of Fat-HA (red) and Bazooka-mCherry (brown) fluorescence along
1043 the normalized AP axis in third instar larval wing pouches. Shaded regions for each
1044 profile represent the standard error of the mean.

1045 (M) Moving line average of Fat-GFP fluorescence along the normalized AP axis of wildtype
1046 and $ds^{33k/UAO71}$ mutant wing pouches from 4-day old larvae. Shaded regions for each
1047 profile represent the standard error of the mean.

1048

1049 **Figure 2 - figure supplement 1. smFISH images of *fat* and *ds* expression in the wing**
1050 **pouch.**

1051 (A) Confocal images of a *ds-GF*P larval wing pouch stained for GFP mRNAs (left) and DAPI
1052 (right). Scale bar is 50 micrometers.

1053 (B) Confocal images of a *fat-GF*P larval wing pouch stained for GFP mRNAs (left) and DAPI
1054 (right). Scale bar is 50 micrometers.

1055

1056 **Figure 2 - figure supplement 2. Methods to measure distributions of Ds-GFP and Fat-GFP.**

1057 (A) Confocal images of a *ds-GF*P larval wing pouch showing GFP fluorescence (left) and
1058 staining of En and Wg proteins (right). Blue and red lines are the AP and DV axes of
1059 symmetry, respectively. Scale bar is 50 micrometers.

1060 (B) Schematic of the wing disc depicting the AP (blue) and DV (red) axes of symmetry.

1061 (C) Representative Ds-GFP fluorescence image in which fluorescence from cells in the disc
1062 proper has been computationally segregated from signal from the peripodial membrane.
1063 Left is a max projection of all sections. Middle is the surface projected signal from the
1064 disc proper. Right is the projected signal from the peripodial membrane.

1065 (D) Confocal images of a *fat-GF*P larval wing pouch showing GFP fluorescence (left) and
1066 staining of En and Wg proteins (right). Blue and red lines are the AP and DV axes of
1067 symmetry, respectively. Scale bar is 50 micrometers.

1068

1069 **Figure 2 - figure supplement 3. Fat expression in *ds* and *fj* mutants.**

1070 (A) Moving line average of Fat-GFP fluorescence along the normalized AP axis. Shown are
1071 profiles from different ages (as indicated) of $ds^{33k/UAO71}$ mutants. Shaded regions for each
1072 profile represent the standard error of the mean.

1073 (B) Moving line average of Fat-GFP fluorescence along the normalized AP axis of $ds^{33k/UAO71}$
1074 mutant wing pouches from WPP and BPP animals. Shaded regions for each profile
1075 represent the standard error of the mean.

1076 (C) Moving line average of Fat-GFP fluorescence along the normalized AP axis of $fj^{d1/p1}$
1077 mutant wing pouches from 4-day old larvae. Shaded regions for each profile represent
1078 the standard error of the mean.

1079

1080 **Figure 3. Ds and Fat expression dynamics correlate with wing pouch volume.**

1081 (A) Wing pouch area of *nub-Gal4* control and *nub>trol*(RNAi) discs from the WPP stage.
1082 Shown are replicates and the mean.

1083 (B) Wing pouch thickness of *nub-Gal4* control and *nub>trol*(RNAi) discs from the WPP
1084 stage. Shown are replicates and the mean.

1085 (C) Wing pouch volume of *nub-Gal4* control and *nub>trol*(RNAi) discs from the WPP stage.
1086 Shown are replicates and the mean.

1087 (D) Moving line average of Ds-GFP fluorescence as a function of position along the AP axis
1088 normalized to the total distance of the axis in *nub-Gal4* control and *nub>trol*(RNAi) WPP
1089 wing pouches. Shaded regions for each profile represent the standard error of the mean.

1090 (E) Moving line average of Fat-GFP fluorescence as a function of position along the AP axis
1091 normalized to the total distance of the axis in *nub-Gal4* control and *nub>trol*(RNAi) WPP
1092 wing pouches. Shaded regions for each profile represent the standard error of the mean.

1093 (F) Confocal image of DAPI-stained nuclei in an *en>RBF* wing pouch. Note the lower
1094 density of nuclei in the P compartment (to the right of the dashed red line). This is due to
1095 the enlarged size of cells in this compartment. Scale bar is 30 micrometers.

1096 (G) The area ratio of P compartment to A compartment in *en-Gal4* control and *en>RBF* wing
1097 pouches from WPP animals. Shown are replicates and the mean.

1098 (H) Moving line average of Ds-GFP fluorescence as a function of position along the AP axis
1099 normalized to the total distance of the axis in *en-Gal4* control and *en>RBF* WPP wing
1100 pouches. Shaded regions for each profile represent the standard error of the mean.

1101 (I) Moving line average of Fat-GFP fluorescence as a function of position along the AP axis
1102 normalized to the total distance of the axis in *en-Gal4* control and *en>RBF* WPP wing
1103 pouches. Shaded regions for each profile represent the standard error of the mean.

1104

1105 **Figure 4. Allometric growth of the wing pouch is altered in *ds* and *fat* mutants.**

1106 (A) Wet-weight of wildtype, *ds*$^{33k/UAO71}$, and *fat*$^{G\text{-}rv/8}$ mutant third instar larvae as a function of
1107 age. Shaded regions represent standard error of the mean in this and the other panels.

1108 (B) Wet-weight of wildtype and mutant animals during early pupariation.

1109 (C) Volume of wildtype and mutant wing pouches as a function of larval age.

1110 (D) Volume of wildtype and mutant wing pouches during early pupariation.

1111 (E) Allometric growth relationship of the wing pouch versus body weight in wildtype and
1112 mutants.

1113

1114 **Figure 4 - figure supplement 1. Allometric growth of the notum-hinge is altered in *ds* and**
1115 ***fat* mutants.**

1116 (A) Area of the wildtype, *ds*$^{33k/UAO71}$, and *fat*$^{G\text{-}rv/8}$ mutant notum-hinge as a function of larval
1117 age. Shaded regions represent standard error of the mean in this and the other panels.

1118 (B) Area of the wildtype and mutant notum-hinge during early pupariation.

1119 (C) Allometric growth relationship of the notum-hinge versus body weight in wildtype and
1120 mutants.

1121

1122 **Figure 5. Autonomous requirements for Fat and Ds in wing pouch growth.**

1123 (A) Schematic of the *nub-Gal4* driver inducing RNAi of *fat* or *ds* in the wing pouch by shRNA
1124 expression.

1125 (B) Wet-weight of *nub-Gal4* control, *nub>ds*(RNAi), *nub>fat*(RNAi), and *nub>ds fat*(RNAi)
1126 third instar larvae as a function of age. Shaded regions represent standard error of the
1127 mean.

1128 (C) Wet-weight of control and RNAi-treated animals during early pupariation. Shaded
1129 regions represent standard error of the mean.

1130 (D) Volume of control and RNAi-treated wing pouches as a function of larval age. Shaded
1131 regions represent standard error of the mean.

1132 (E) Volume of control and RNAi-treated wing pouches during early pupariation. Shaded
1133 regions represent standard error of the mean.

1134 (F) Allometric growth relationship of the wing pouch versus body weight in control and RNAi-
1135 treated animals.

1136 (G) Schematic of the *ap-Gal4* driver inducing RNAi of *ds* in the D compartment by shRNA
1137 expression.

1138 (H) Ratio of D compartment area to V compartment area in *ap-Gal4* control and
1139 *ap>ds*(RNAi) wing pouches from WPP animals. Shown are replicate measurements and
1140 their mean.

1141 (I) Wing pouch area of *ap-Gal4* control and *ap>ds*(RNAi) WPP animals. Shown are
1142 replicate measurements and their mean. The area is normalized to the average of *ap-*
1143 *Gal4* controls.

1144 (J) Cell number in the D compartment of the wing pouch of *ap-Gal4* control and
1145 *ap>ds*(RNAi) WPP animals. Shown are replicate measurements and their mean. The
1146 cell number is normalized to the average of *ap-Gal4* controls.

1147 (K) Average cell size (apical area) in the D compartment of the wing pouch of *ap-Gal4*
1148 control and *ap>ds*(RNAi) WPP animals. Shown are replicate measurements and their
1149 mean. The cell size is normalized to the average of *ap-Gal4* controls.

1150 (L) Schematic of the *en-Gal4* driver inducing RNAi of *ds* and fat in the P compartment by
1151 shRNA expression.

1152 (M) Ratio of P compartment area to A compartment area in *en-Gal4* control, *en>fat*(RNAi),
1153 *en>ds*(RNAi), and *en>fat ds*(RNAi) wing pouches from WPP animals. Shown are
1154 replicate measurements and their mean.

1155 (N) Wing pouch area of *en-Gal4* control and RNAi knockdown WPP animals. Shown are
1156 replicate measurements and their mean. The area is normalized to the average of *en-*
1157 *Gal4* controls.

1158 Samples that were significantly different are marked with asterisks (*, $p < 0.05$; **, $p < 0.01$; ***,
1159 $p < 0.001$; ****, $p < 0.0001$).

1160

1161 **Figure 5 - figure supplement 1. RNAi effectively knocks down *fat* and *ds* expression.** All
1162 panels show confocal images of third instar larval wing discs. Scale bars are 50 micrometers.

1163 (A) Endogenously expressed Ds-GFP.

1164 (B) Anti-Ds staining of *nub>ds*(RNAi) disc. Ds expression in the peripodial membrane and
1165 notum remains unchanged.

1166 (C) Endogenously expressed Fat-GFP.

1167 (D) Fat-GFP expression in a *nub>fat*(RNAi) disc. Fat expression in the peripodial membrane
1168 and notum remains unchanged.

1169 (E) Ds-GFP expression in an *ap>ds*(RNAi) disc (left). Ds expression in the ventral
1170 compartment remains unchanged. E-cadherin-mCherry is used for cell segmentation
1171 (right). The compartment boundary is shown in yellow.

1172 (F) Ds-GFP expression in an *en>ds*(RNAi) disc. Ds expression in the anterior compartment
1173 remains unchanged. The compartment boundary is shown in yellow.

1174 (G) Fat-GFP expression in an *en>fat*(RNAi) disc. Fat expression in the anterior compartment
1175 remains unchanged. The compartment boundary is shown in yellow.

1176

1177 **Figure 5 - figure supplement 2. Growth of the notum-hinge when *fat* and *ds* are knocked**
1178 **down in the wing pouch.**

1179 (A) Notum-hinge area of *nub-Gal4* control, *nub>ds*(RNAi), *nub>fat*(RNAi), and *nub>ds*
1180 *fat*(RNAi) as a function of larval age. Shaded regions represent standard error of the
1181 mean in this and the other panels.

1182 (B) Notum-hinge area of control and RNAi-treated animals during early pupariation.

1183 (C) Allometric growth relationship of the notum-hinge versus body weight in control and
1184 RNAi-treated animals.

1185

1186 **Figure 6. Scaling of cell cycle duration with wing size is regulated by Ds and Fat.** The
1187 average cell cycle time for wing pouch cells is plotted against wing pouch volume for wing discs

sampled over 1.5 days of larval growth. Solid lines show the linear regression model, and dotted lines show the 95% confidence intervals of the fit.

(A) *nub-gal4* control.

(B) *nub>ds*(RNAi) and *nub-gal4* control.

(C) *nub>fat*(RNAi) and *nub-gal4* control.

(D) *nub>ds fat*(RNAi) and *nub-gal4* control.

(E) *nub>ds*(RNAi) and *nub>ds fat*(RNAi).

Figure 6 - figure supplement 1. Measurement of length of M phase in wing pouch cells. Third instar wing discs expressing E-cadherin-GFP were dissected and cultured *ex vivo* as described by Gallagher et al. (2022). Each disc was successively imaged by microscopy over a 2-hr period, with an image frame time interval of 5 min.

(A) A cell undergoing mitosis starting at t = 5 minutes. Cytokinesis is completed at t = 25 minutes. The beginning of mitosis is marked by the first detectable increase in a cell's apical area. The cell expands and becomes circular, after which mitosis completes and the cell contracts in area as it divides. The end of cytokinesis is marked by the last detectable decrease in daughter cell apical area.

(B) Histogram of M phase times for 33 wing pouch cells. The mean time is 20.5 min.

Figure 6 - supplement table 1. Summary statistics of linear regression analysis.

Figure 7. The endogenous graded distribution of Fat and Ds is not essential for controlling growth rate of the wing pouch.

(A) *nub-Gal4* driving expression of *UAS-GFP-NLS* along the AP axis of symmetry in the wing pouch. This demonstrates the graded expression of genes transcribed by *nub-Gal4*. Shown are moving line averages for larval and pupal wing pouches. Shaded regions represent standard error of the mean.

(B) Schematic of the *nub-Gal4* driver expressing *ds* under the UAS promoter.

(C) Moving line average of Ds protein stained with anti-Ds as a function of position along the AP axis and normalized to the total distance of the axis. Shown are staged larval wing pouches from *nub>ds* animals. This measurement also detects expression from the endogenous *ds* gene. Shaded regions for each profile represent the standard error of the mean.

(D) Moving line average of Ds protein stained with anti-Ds as a function of position along the DV axis and normalized to the total distance of the axis. Shown are staged larval wing pouches from *nub>ds* animals. Shaded regions for each profile represent the standard error of the mean.

(E) Moving line average of Fat-GFP fluorescence as a function of position along the AP axis and normalized to the total distance of the axis. Shown are staged larval and pupal wing pouches from *nub>ds* animals. Shaded regions for each profile represent the standard error of the mean.

(F) Schematic of the *nub-Gal4* driver expressing *fat-HA* under the UAS promoter.

(G) Moving line average of transgenic Fat-HA protein stained with anti-HA as a function of position along the AP axis and normalized to the total distance of the axis. Shown are staged larval and pupal wing pouches from *nub>fat-HA; fat-GFP* animals. This measurement does not detect expression from the endogenous *fat-GFP* gene. Shaded regions for each profile represent the standard error of the mean.

(H) Moving line average of endogenous Fat-GFP fluorescence as a function of position along the AP axis and normalized to the total distance of the axis. Shown are staged larval and pupal wing pouches from *nub>fat-HA; fat-GFP* animals. Shaded regions for each profile represent the standard error of the mean.

(I) The average cell cycle time for wing pouch cells plotted against wing pouch volume for wing discs from *nub-Gal4* control animals and *nub>fat-HA; fat-GFP* animals. Solid lines show the linear regression model, and dotted lines show the 95% confidence intervals for the fit. There is no significant difference between the slopes (p = 0.65).

Figure 7 - figure supplement 1. Reversal of the Ds expression gradient does not affect growth.

(A) Confocal images of a *nub>ds; fat-GFP* third instar larval wing disc showing Fat-GFP fluorescence (left), anti-Ds fluorescence (center), and anti-Wg / anti-En fluorescence (right). The AP (blue) and DV (red) axes are shown. Scale bar is 50 micrometers.

(B) Wet-weight of *nub-Gal4* control and *nub>ds* third instar larvae as a function of age. Shaded regions represent standard error of the mean.

(C) Wet-weight of *nub-Gal4* control and *nub>ds* animals during early pupariation. Shaded regions represent standard error of the mean.

(D) Volume of *nub-Gal4* control and *nub>ds* larval wing pouches as a function of age. Shaded regions represent standard error of the mean.

(E) Volume of *nub-Gal4* control and *nub>ds* wing pouches during early pupariation. Shaded regions represent standard error of the mean.

Figure 7 - figure supplement 2. Disruption of Fat gradient dynamics has no detectable effect on wing pouch growth.

(A) Confocal images of a *nub>fat-HA; fat-GFP* third instar larval wing disc showing Fat-GFP fluorescence (left), anti-HA fluorescence (center), and anti-Wg / anti-En fluorescence (right). The AP (blue) and DV (red) axes are shown. Scale bar is 50 micrometers.

(B) Volume of WPP wing pouches from *nub-Gal4* control and *nub>fat-HA; fat-GFP* animals. There is no significant difference between the two groups as determined by a t-test.

Figure 1

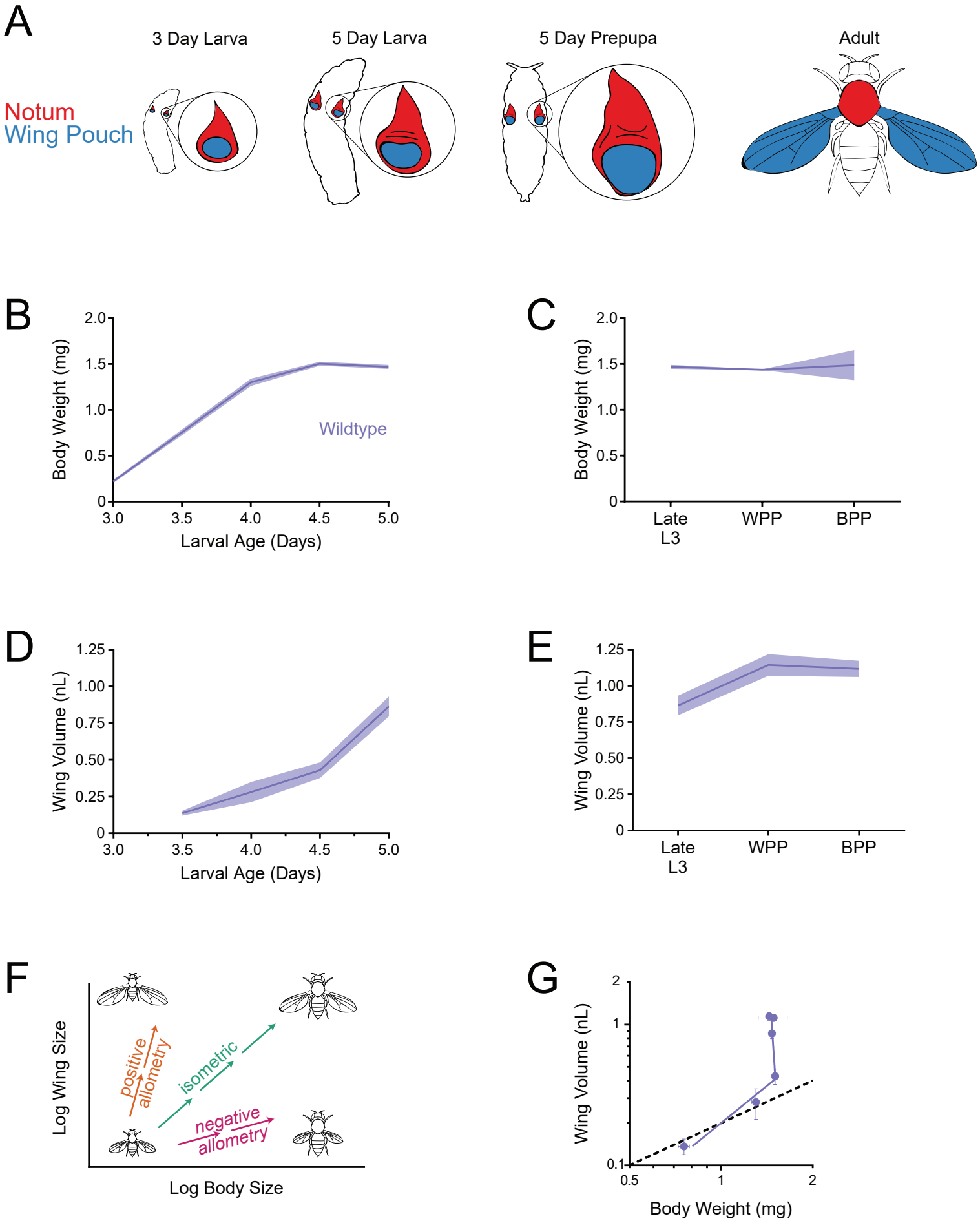
A
3 Day Larva
5 Day Larva
5 Day Prepupa
Adult
Notum
Wing Pouch
B
Body Weight (mg)
Larval Age (Days)
Wildtype
C
Body Weight (mg)
Late L3
WPP
BPP
D
Wing Volume (nL)
Larval Age (Days)
E
Wing Volume (nL)
Late L3
WPP
BPP
F
Log Wing Size
Log Body Size
positive allometry
isometric
negative allometry
G
Wing Volume (nL)
Body Weight (mg)

Figure 1 - figure supplement 1

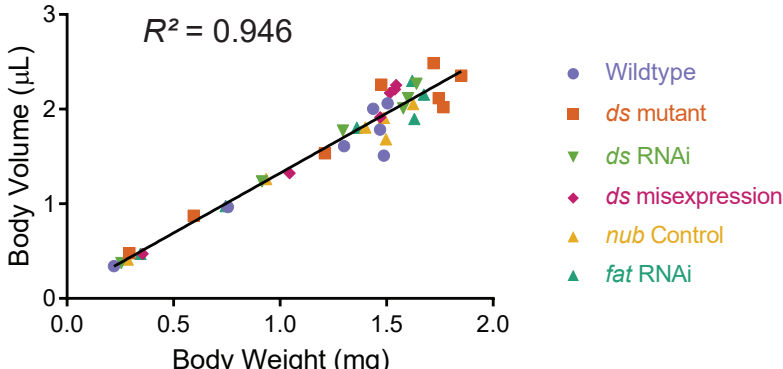

Figure 1 - figure supplement 2

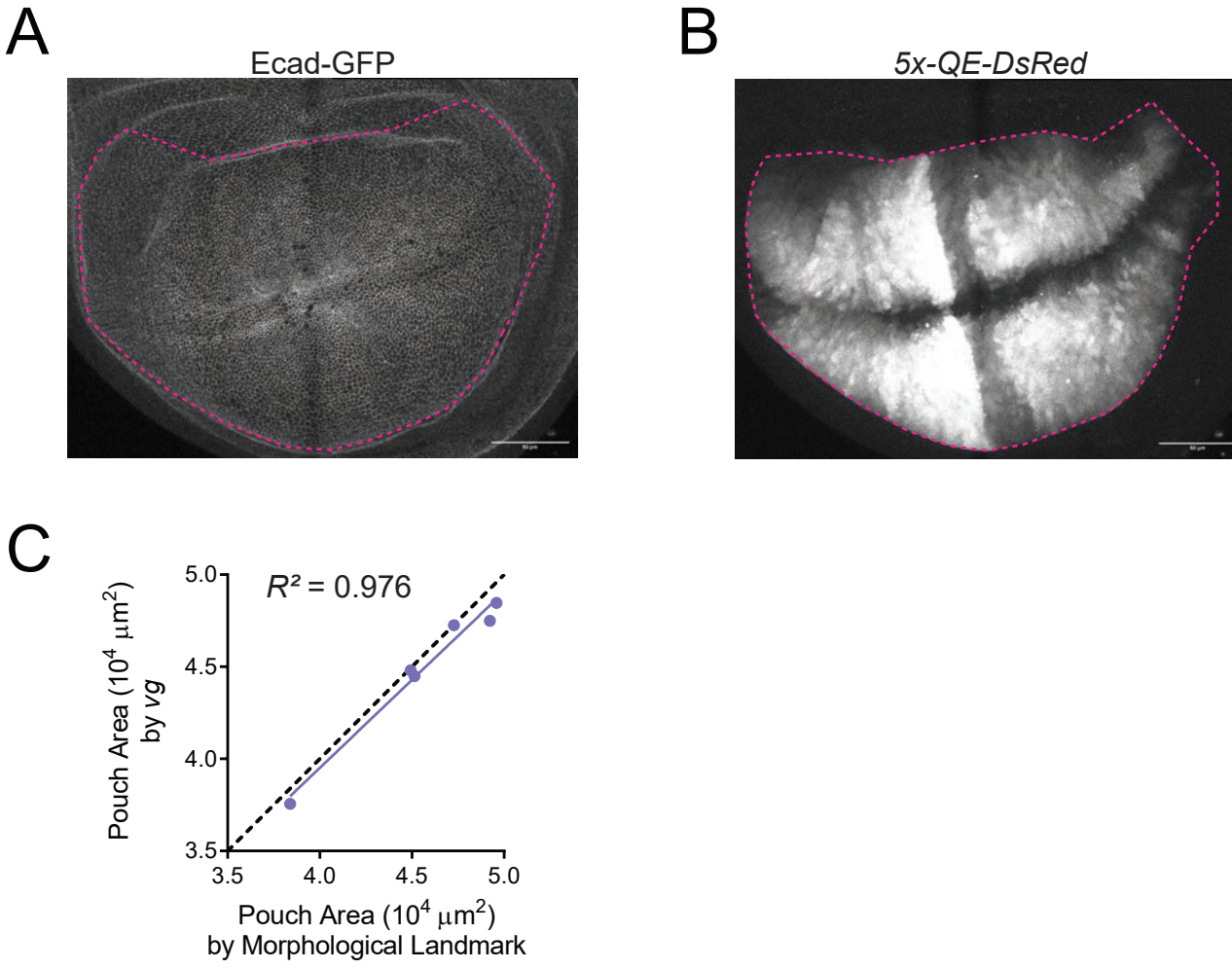

Figure 1 - figure supplement 3

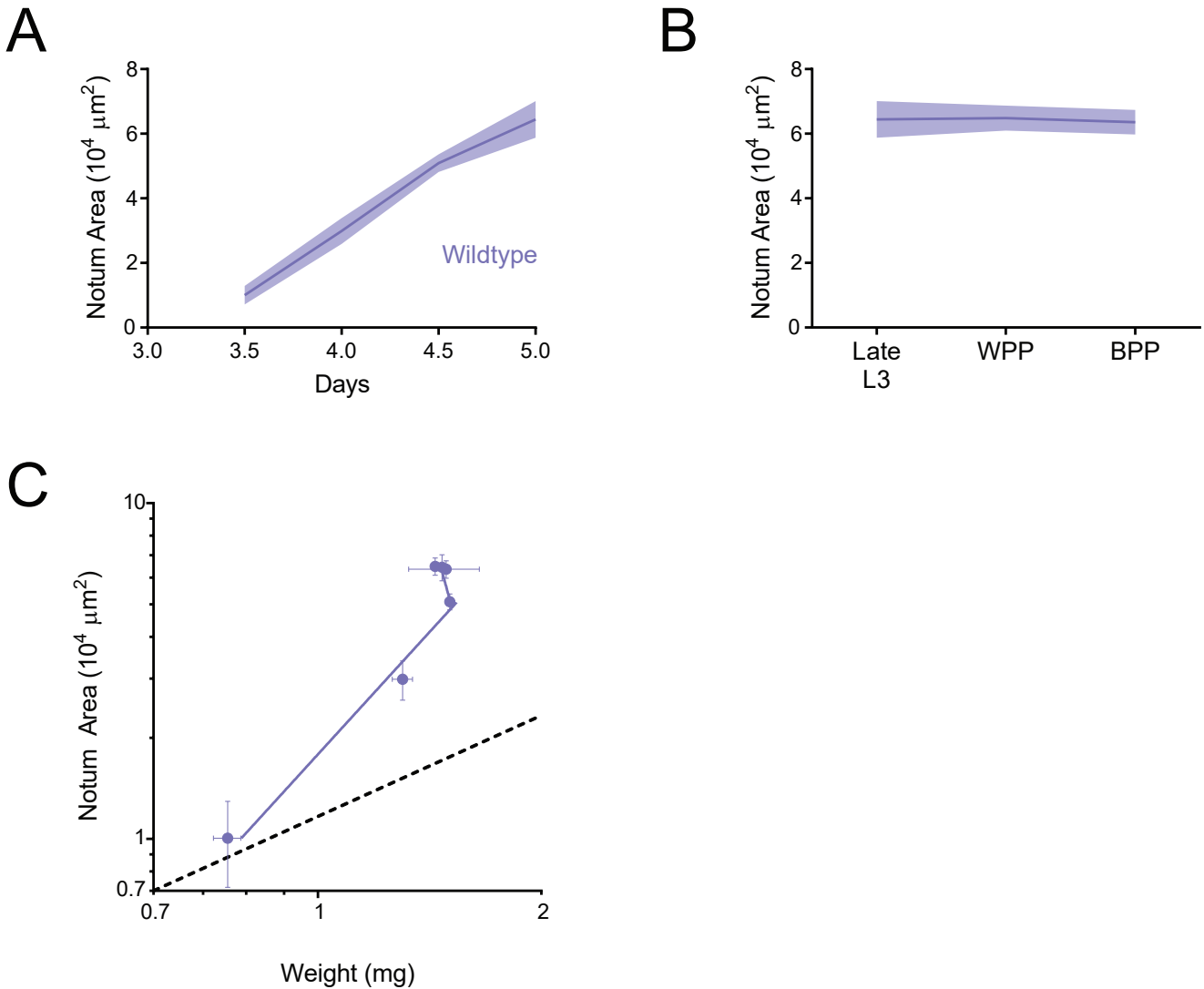

Figure 1 - figure supplement 4

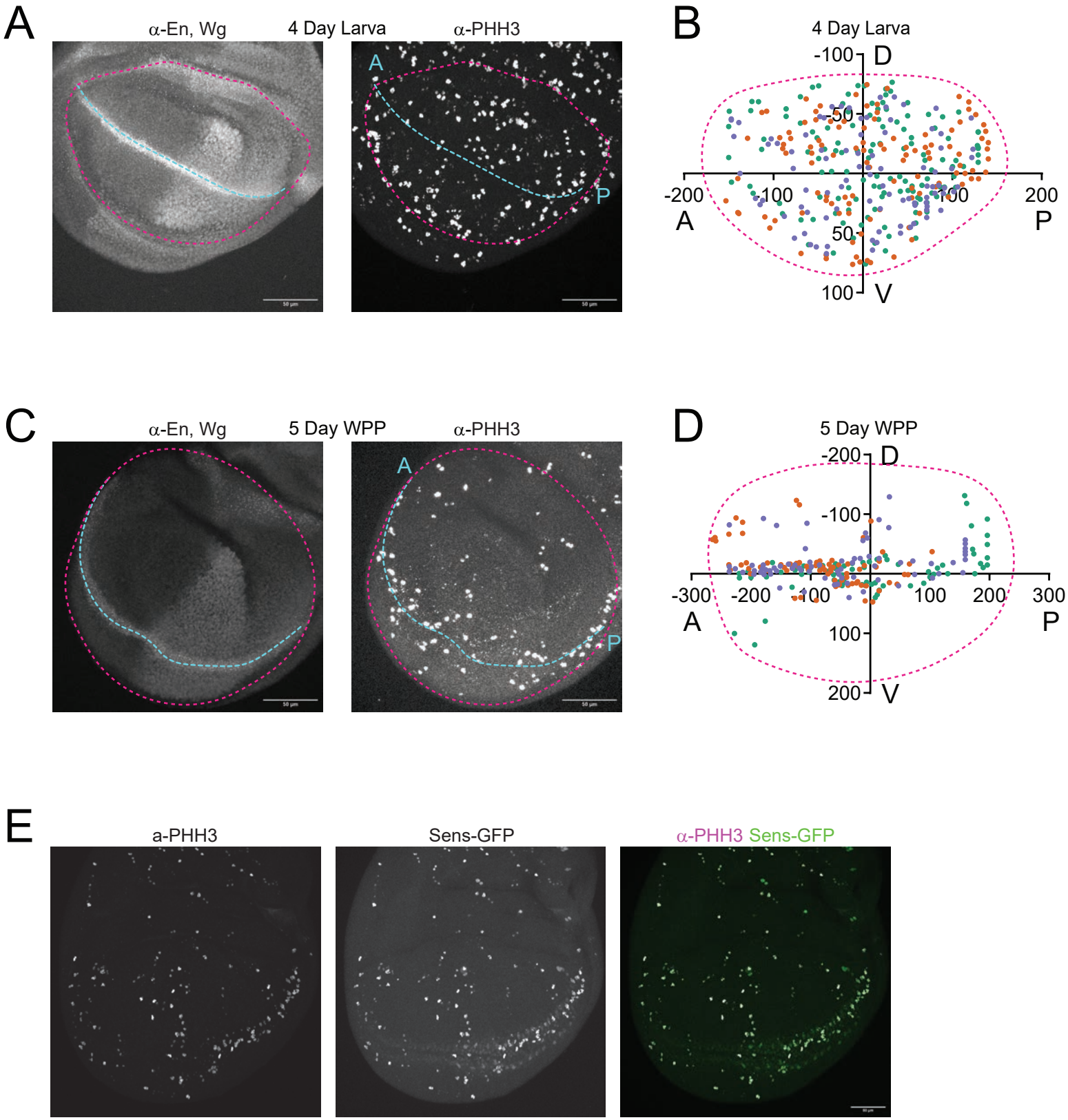

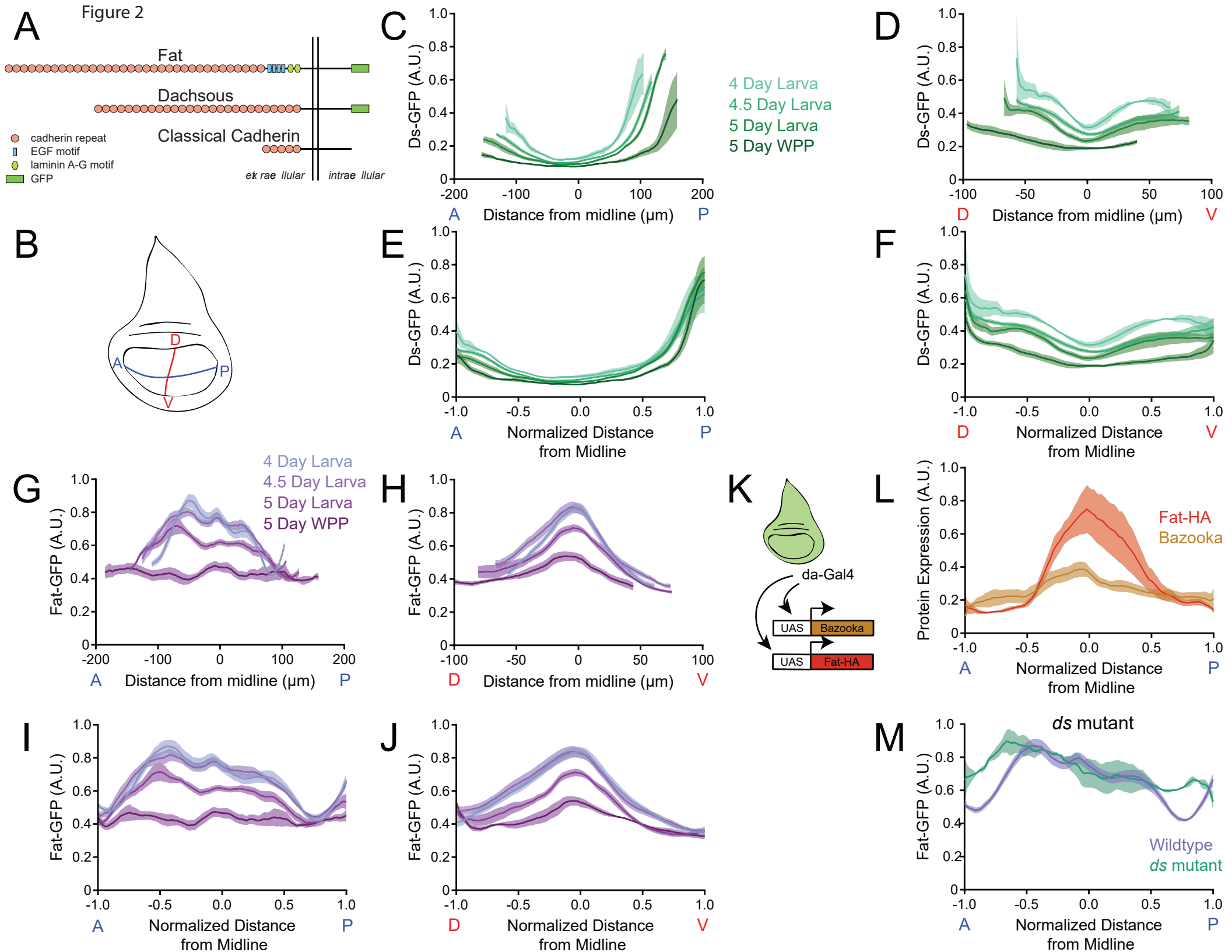
Figure 2
A
Fat
Dachsous
Classical Cadherin
cadherin repeat
EGF motif
laminin A-G motif
GFP
ek rae llular
intrae llular
B
D
A
P
V
C
Ds-GFP (A.U.)
Distance from midline (μm)
A
P
4 Day Larva
4.5 Day Larva
5 Day Larva
5 Day WPP
D
Ds-GFP (A.U.)
Distance from midline (μm)
D
V
E
Ds-GFP (A.U.)
Normalized Distance from Midline
A
P
F
Ds-GFP (A.U.)
Normalized Distance from Midline
D
V
G
Fat-GFP (A.U.)
Distance from midline (μm)
A
P
4 Day Larva
4.5 Day Larva
5 Day Larva
5 Day WPP
H
Fat-GFP (A.U.)
Distance from midline (μm)
D
V
K
da-Gal4
UAS
Bazooka
UAS
Fat-HA
L
Protein Expression (A.U.)
Fat-HA
Bazooka
Normalized Distance from Midline
A
P
I
Fat-GFP (A.U.)
Normalized Distance from Midline
A
P
J
Fat-GFP (A.U.)
Normalized Distance from Midline
D
V
M
ds mutant
Fat-GFP (A.U.)
Wildtype
ds mutant
Normalized Distance from Midline
A
P

Figure 2 - figure supplement 1

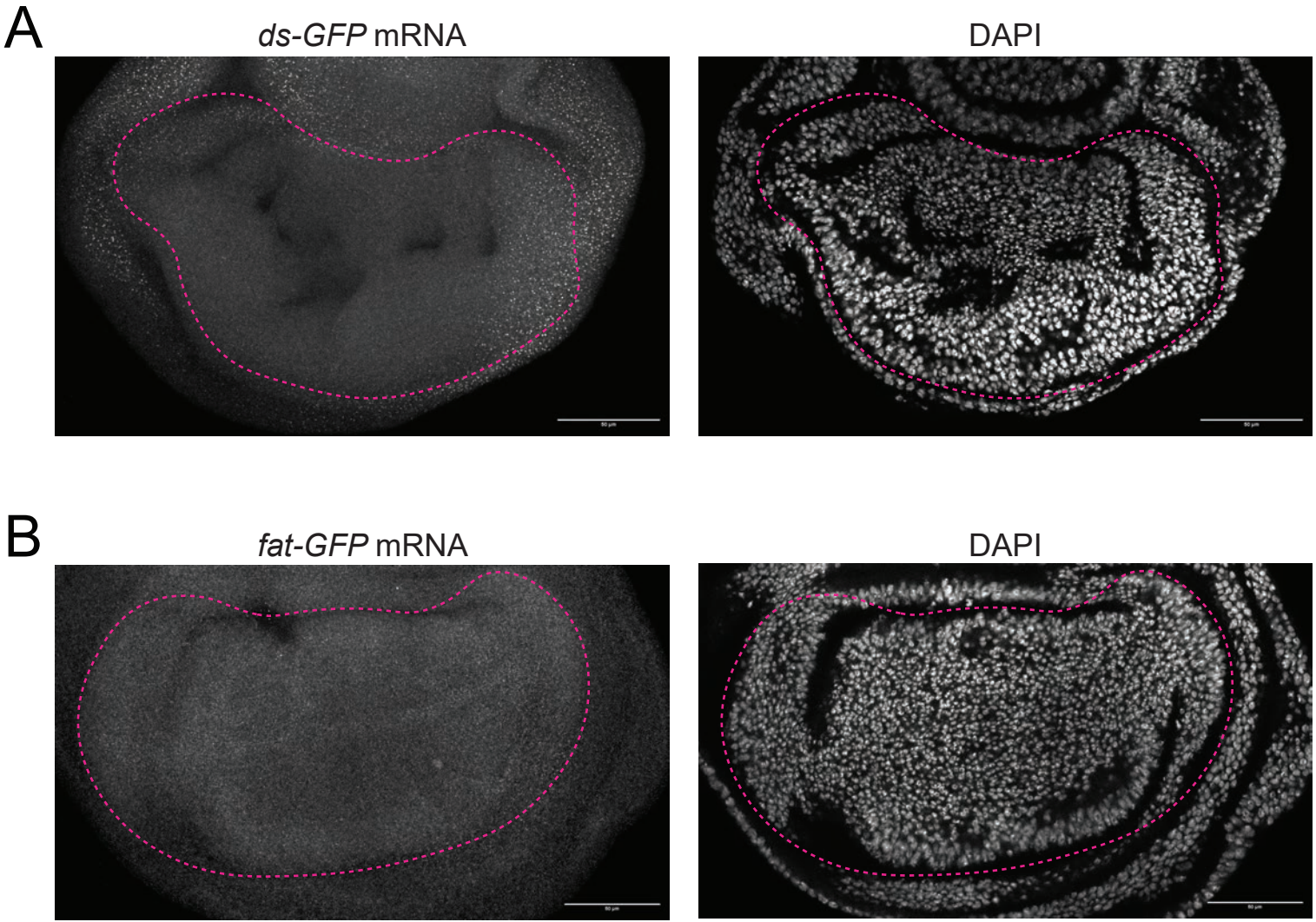

Figure 2 - figure supplement 2

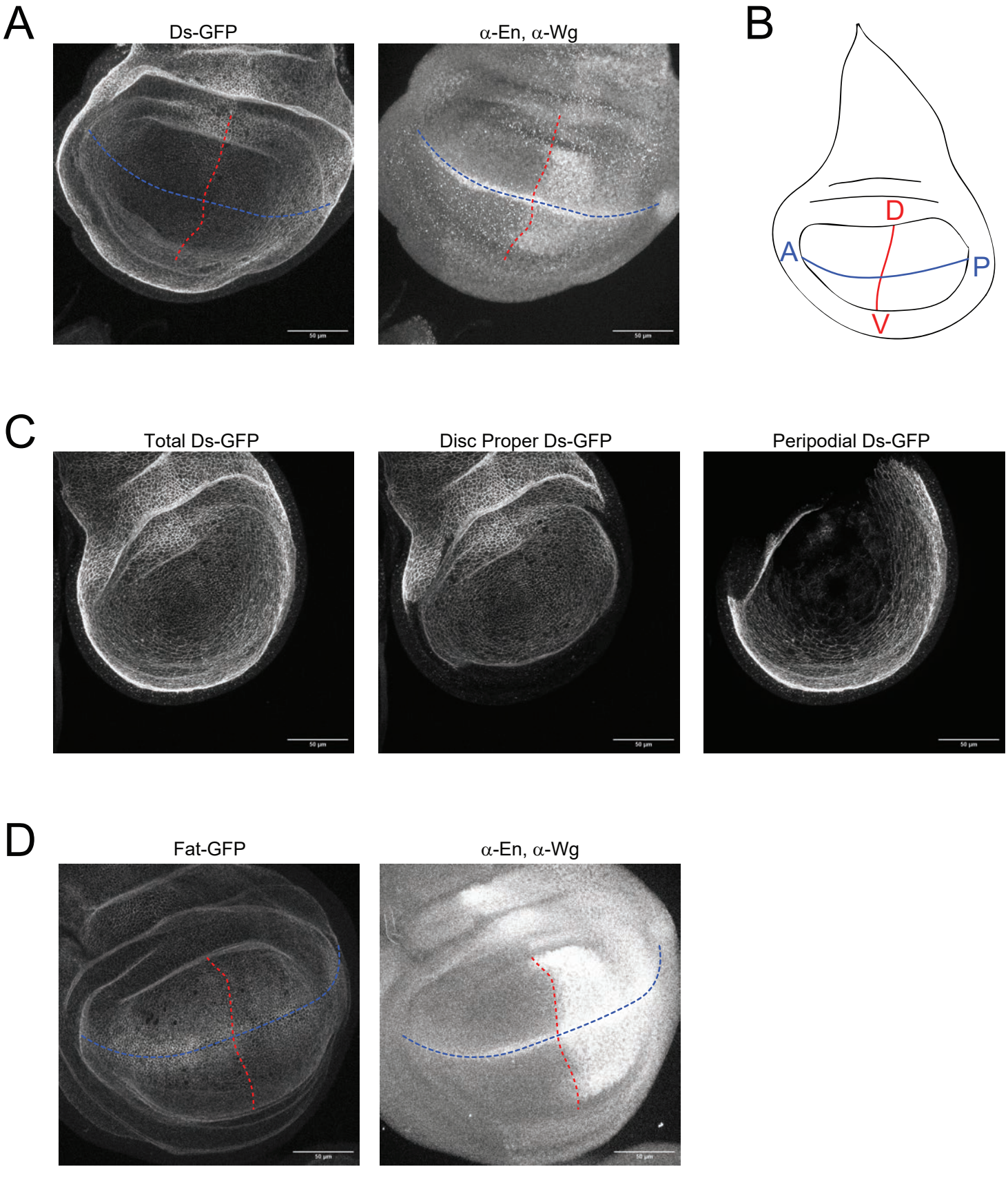

Figure 2 - figure supplement 3

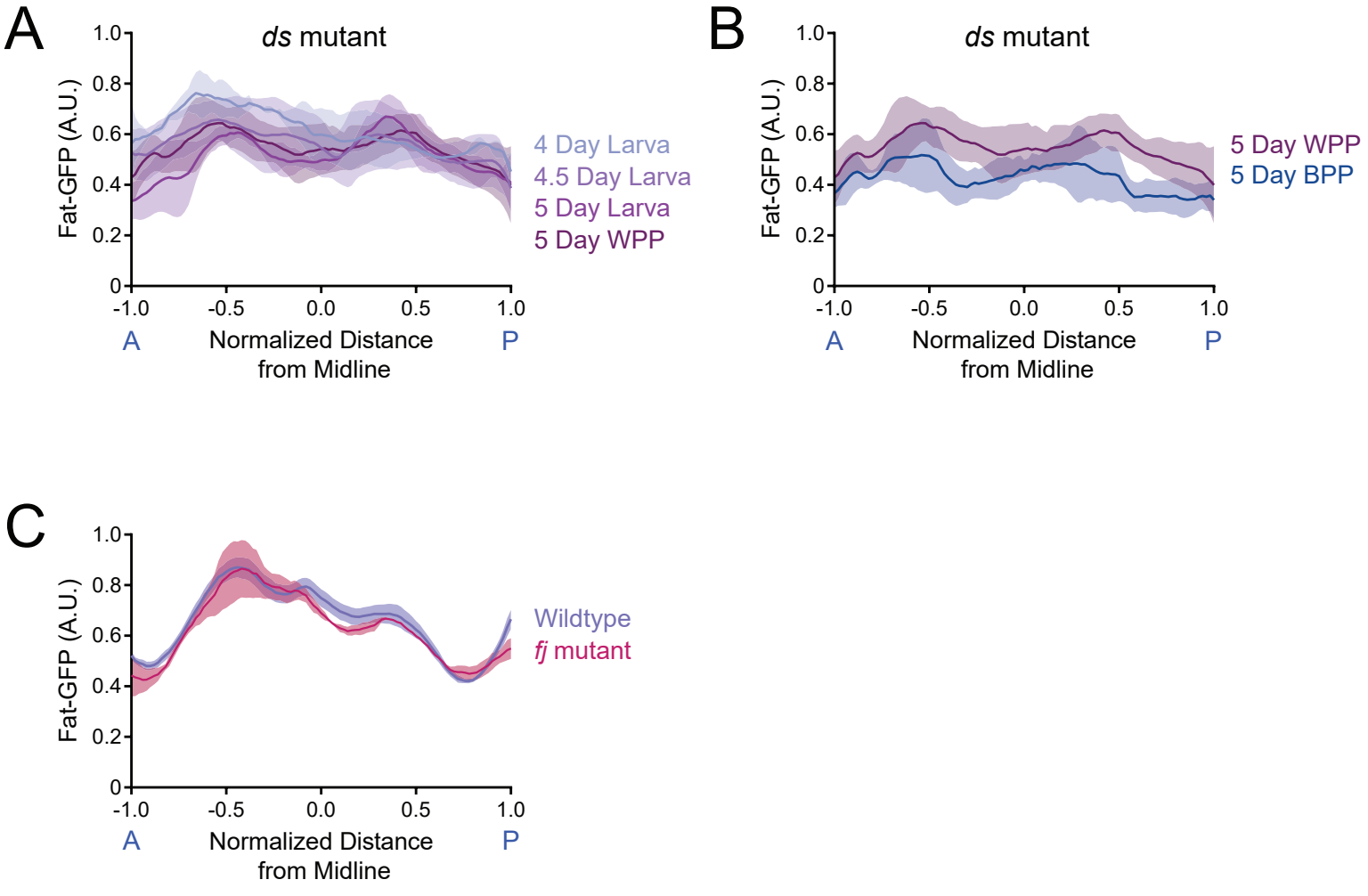

Figure 3

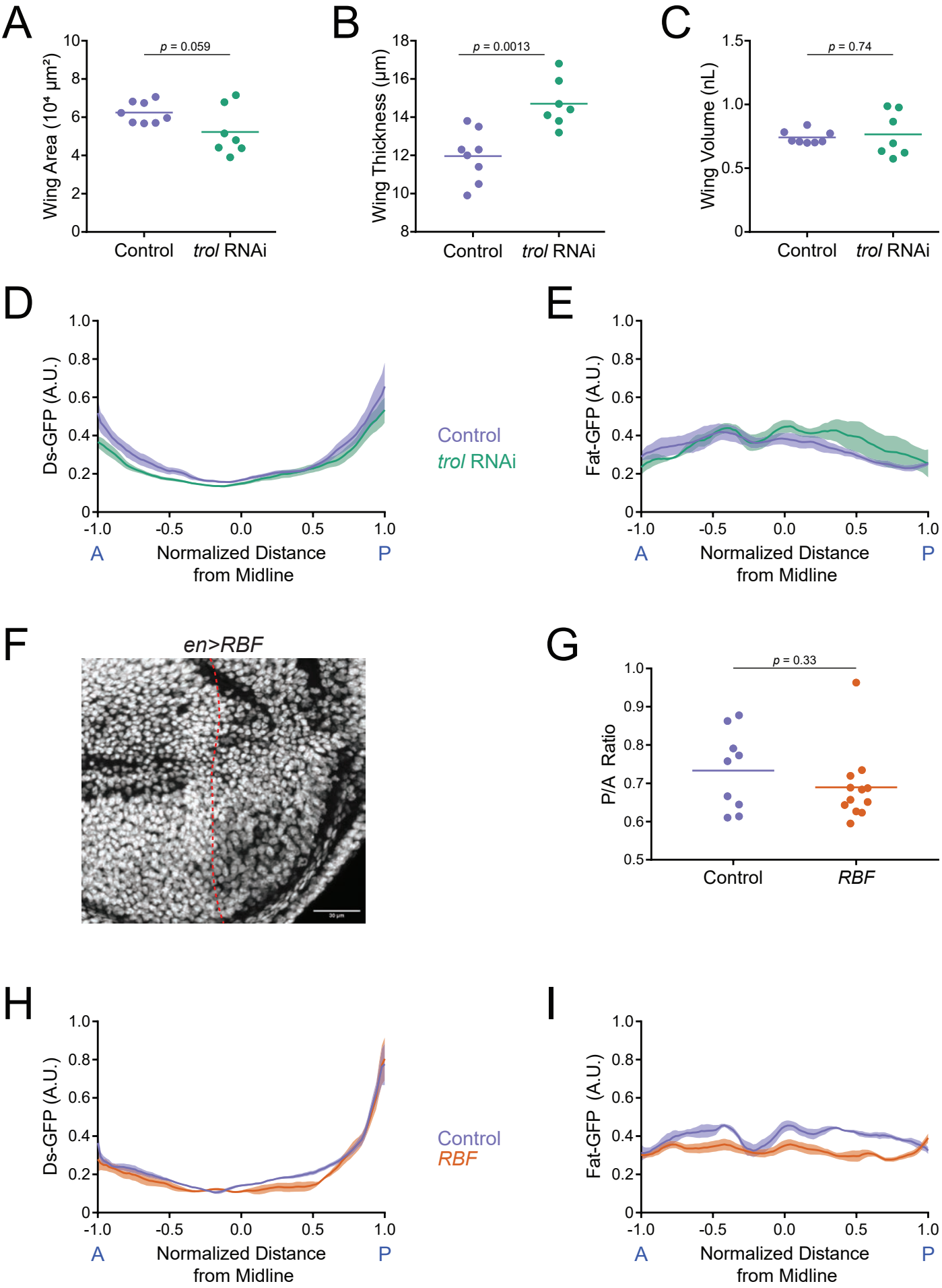
A
Wing Area (10⁴ µm²)
p = 0.059
Control
trol RNAi
B
Wing Thickness (µm)
p = 0.0013
Control
trol RNAi
C
Wing Volume (nL)
p = 0.74
Control
trol RNAi
D
Ds-GFP (A.U.)
Control
trol RNAi
A
Normalized Distance from Midline
P
E
Fat-GFP (A.U.)
A
Normalized Distance from Midline
P
F
en>RBF
G
P/A Ratio
p = 0.33
Control
RBF
H
Ds-GFP (A.U.)
Control
RBF
A
Normalized Distance from Midline
P
I
Fat-GFP (A.U.)
A
Normalized Distance from Midline
P

Figure 4

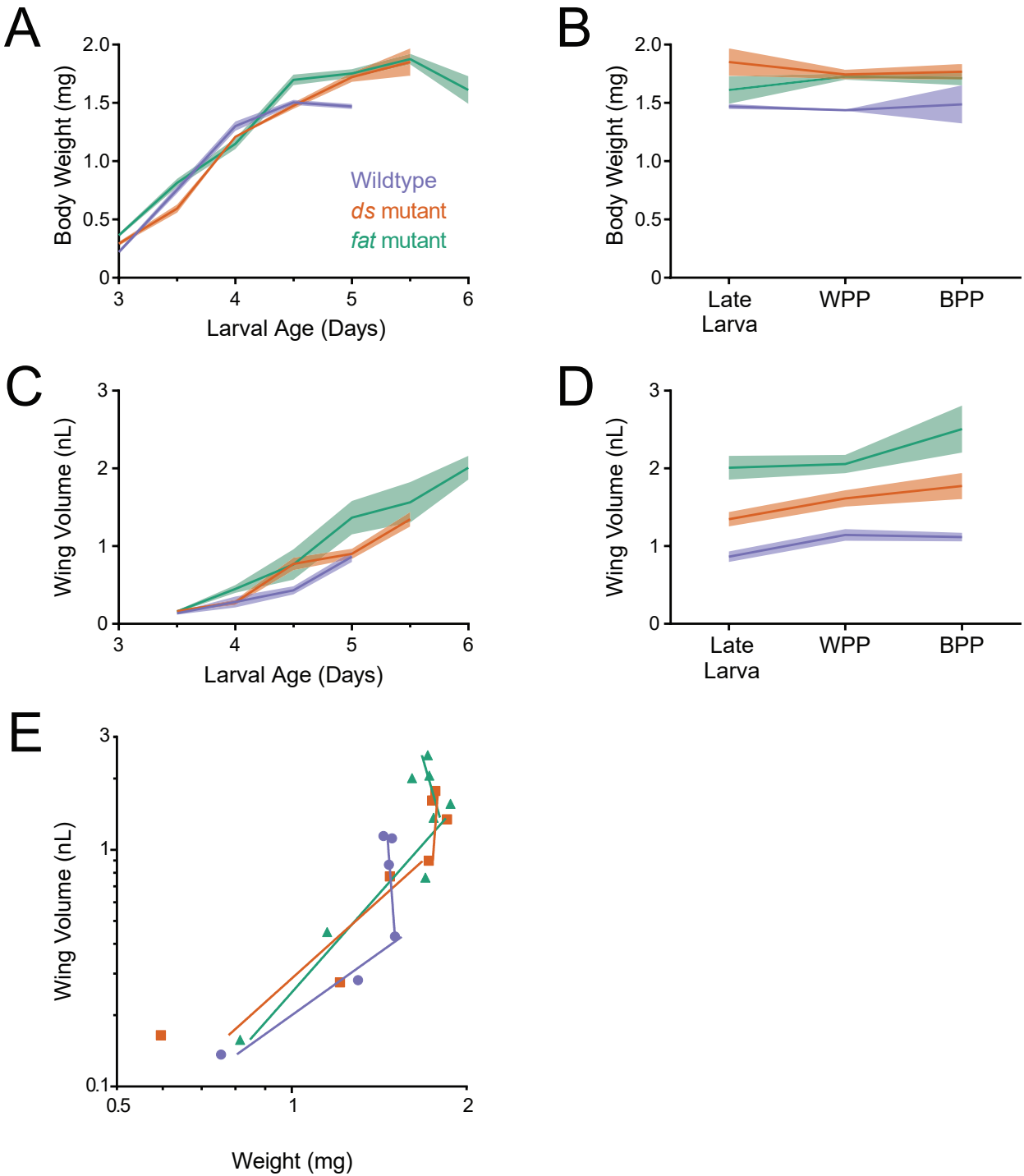
A
Body Weight (mg)
2.0
1.5
1.0
0.5
0
3
4
5
6
Larval Age (Days)
Wildtype
ds mutant
fat mutant
B
Body Weight (mg)
2.0
1.5
1.0
0.5
0
Late Larva
WPP
BPP
C
Wing Volume (nL)
3
2
1
0
3
4
5
6
Larval Age (Days)
D
Wing Volume (nL)
3
2
1
0
Late Larva
WPP
BPP
E
Wing Volume (nL)
3
1
0.1
0.5
1
2
Weight (mg)

Figure 4 - figure supplement 1

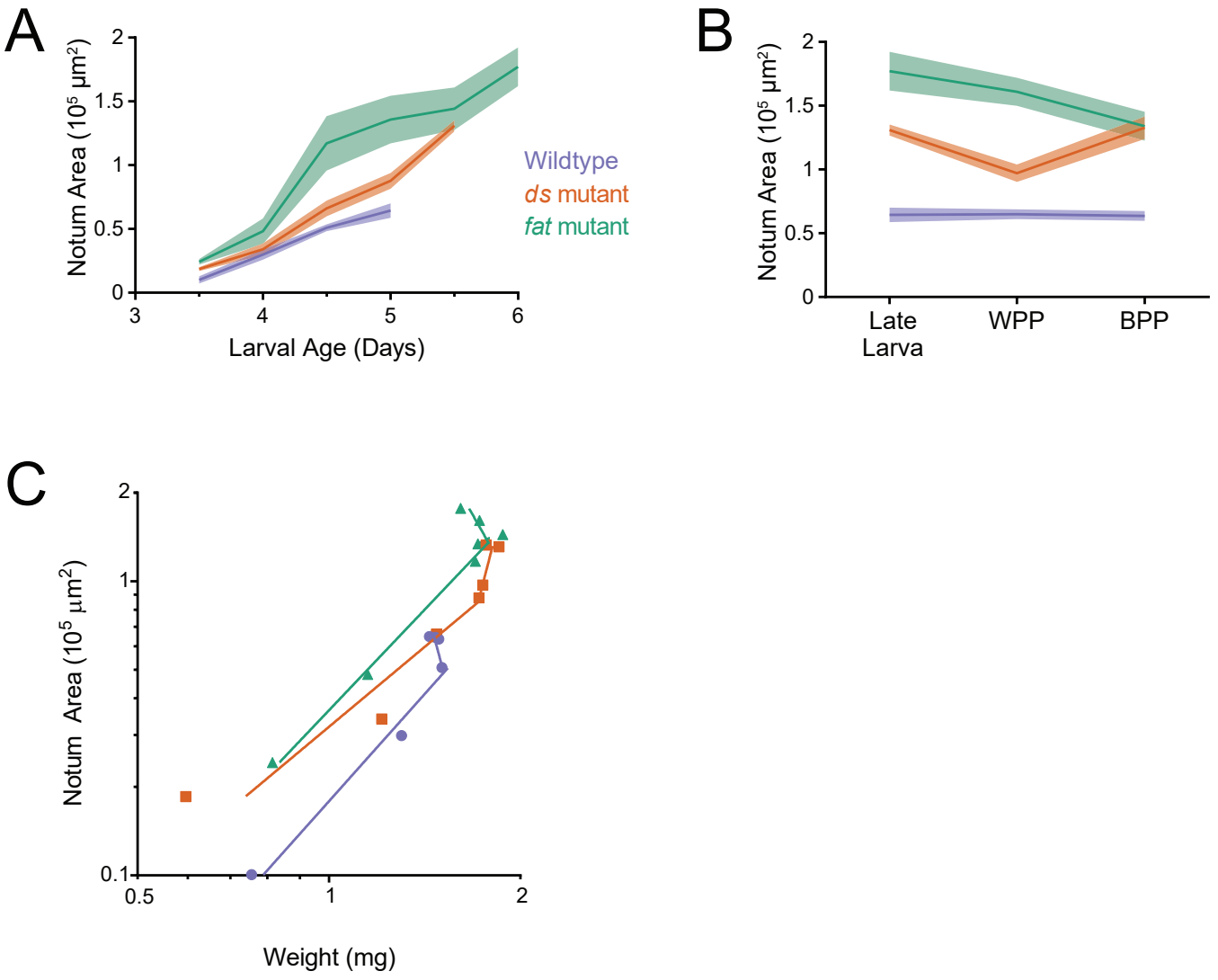

Figure 5

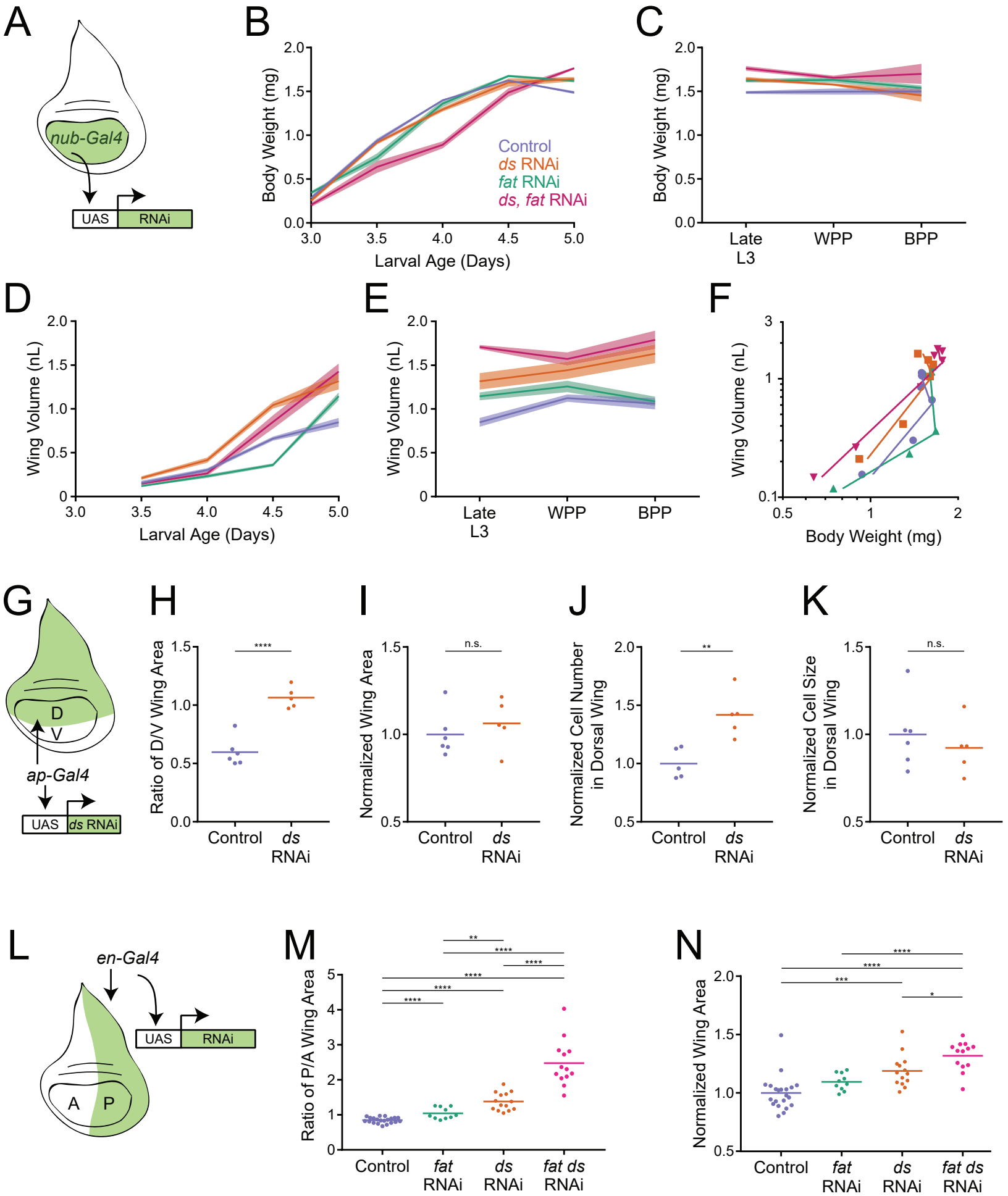
A
nub-Gal4
UAS
RNAi
B
Body Weight (mg)
Larval Age (Days)
Control
ds RNAi
fat RNAi
ds, fat RNAi
C
Body Weight (mg)
Late L3
WPP
BPP
D
Wing Volume (nL)
Larval Age (Days)
E
Wing Volume (nL)
Late L3
WPP
BPP
F
Wing Volume (nL)
Body Weight (mg)
G
D
V
ap-Gal4
UAS
ds RNAi
H
Ratio of D/V Wing Area
****
Control
ds RNAi
I
Normalized Wing Area
n.s.
Control
ds RNAi
J
Normalized Cell Number in Dorsal Wing
**
Control
ds RNAi
K
Normalized Cell Size in Dorsal Wing
n.s.
Control
ds RNAi
L
en-Gal4
UAS
RNAi
A
P
M
Ratio of P/A Wing Area
Control
fat RNAi
ds RNAi
fat ds RNAi
N
Normalized Wing Area
Control
fat RNAi
ds RNAi
fat ds RNAi

Figure 5 - figure supplement 1

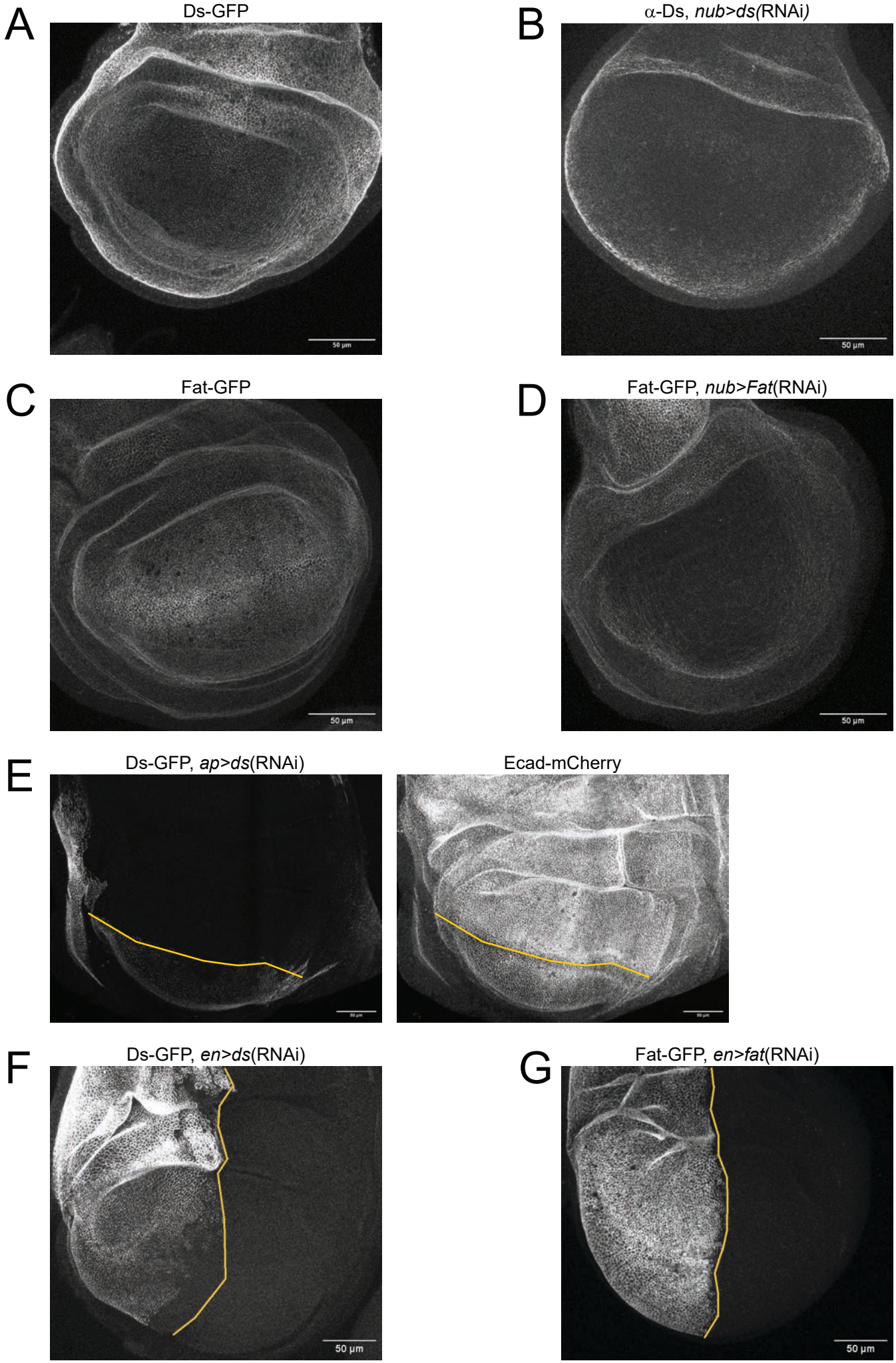

Figure 5 - figure supplement 2

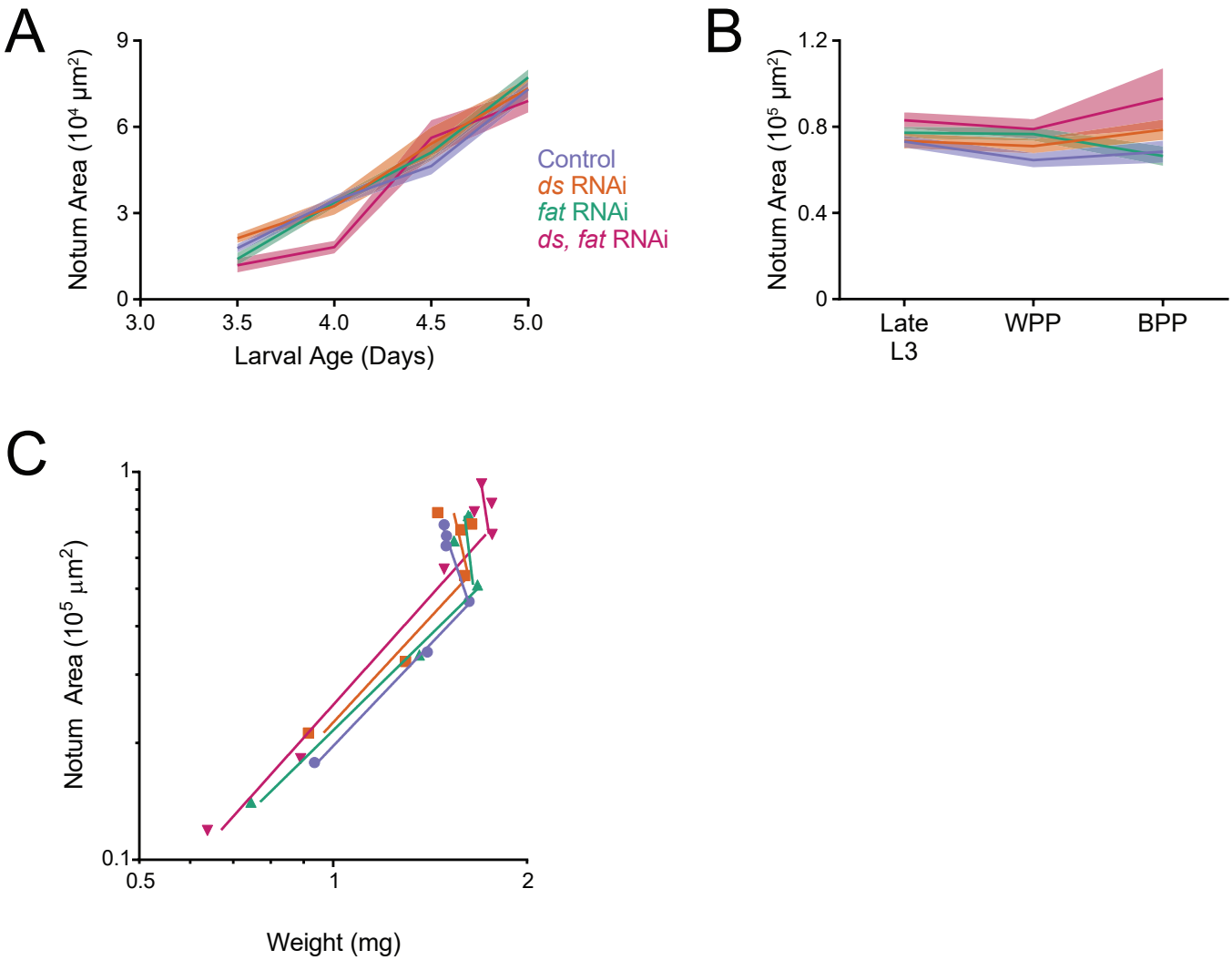

Figure 6

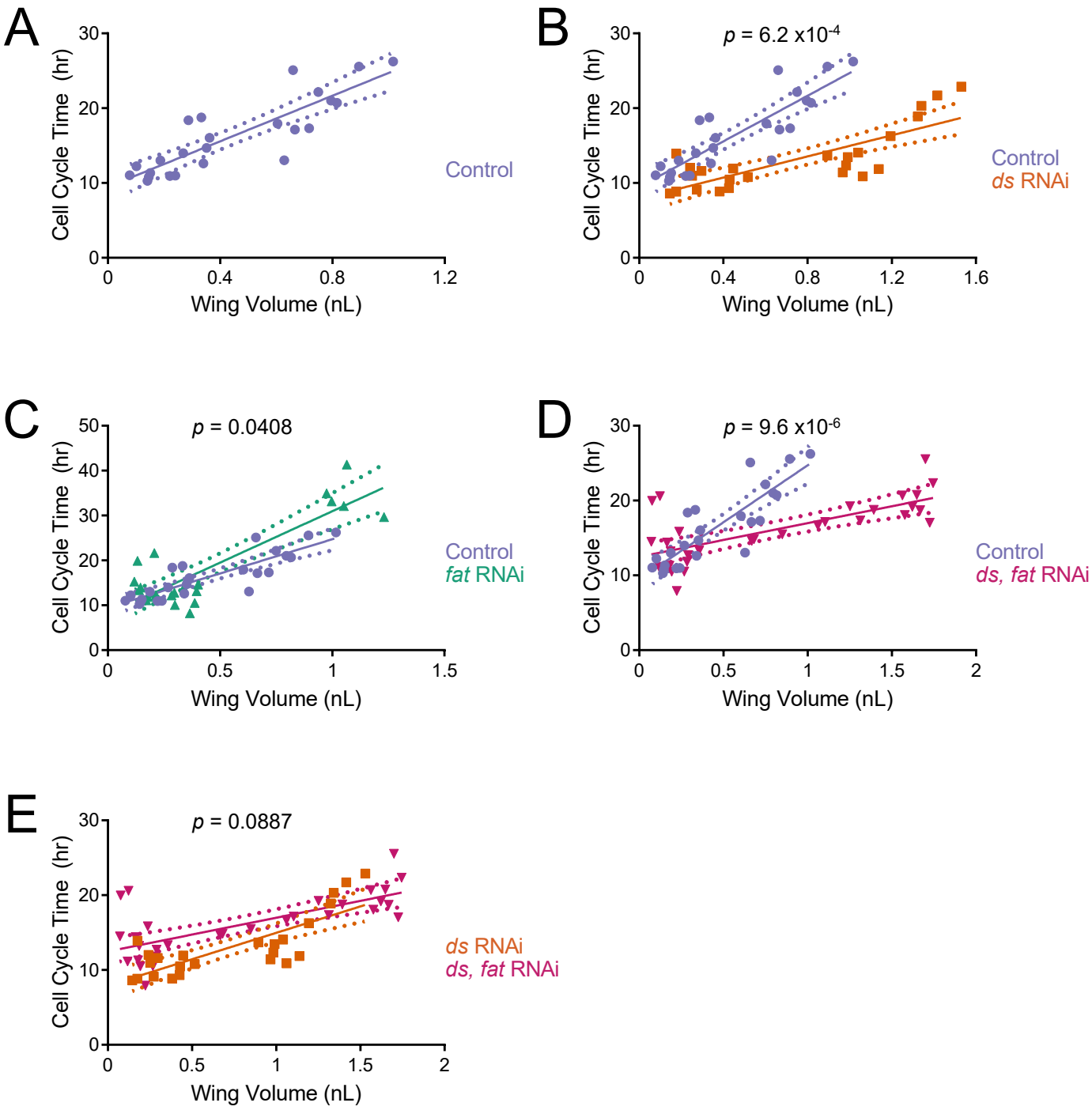
A
Cell Cycle Time (hr)
Wing Volume (nL)
Control
B
p = 6.2 x10-4
Control
ds RNAi
C
p = 0.0408
Control
fat RNAi
D
p = 9.6 x10-6
Control
ds, fat RNAi
E
p = 0.0887
ds RNAi
ds, fat RNAi

Figure 6 - figure supplement 1

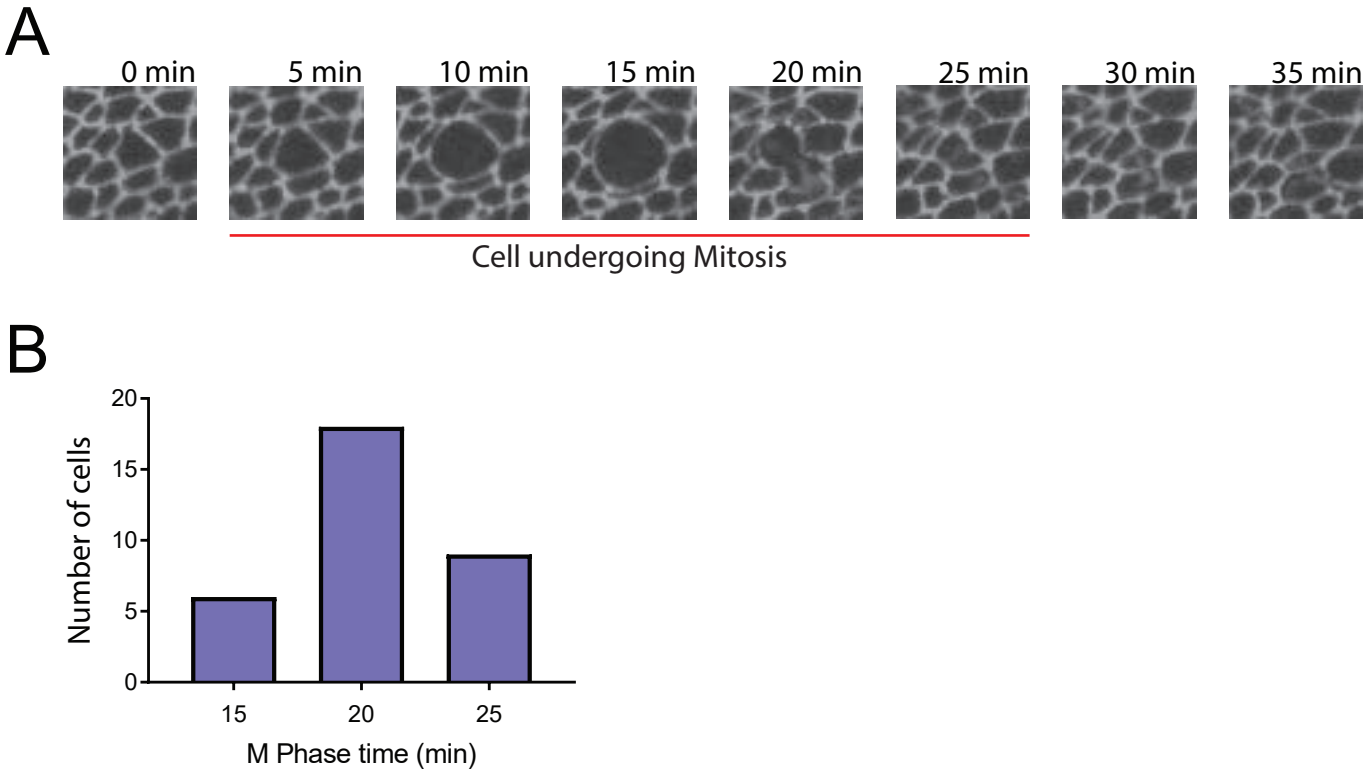

Figure 6 - supplement table 1

	$Time_{Cell\ Cycle} = \beta_0 + \beta_1 \times Volume$				different from control		different from *nub>ds* (RNAi)	
Genotype	β_0	β_1	R^2	*p*	*p* of intercept	*p* of slope	*p* of intercept	*p* of slope
nub-Gal4	9.480 +- 1.011	15.231+- 1.913	0.74	6.38E-08				
nub>ds (RNAi)	7.904 +- 0.992	7.060 +- 1.150	0.63	3.50E-06	0.272	0.00062		
nub>fat (RNAi)	8.049 +- 1.540	22.907 +- 2.850	0.75	5.46E-08	0.465	0.0408		
nub>ds fat (RNAi)	12.4780 +- 0.858	4.507 +- 0.833	0.51	9.00E-06	0.0309	9.57E-06	0.00132	0.0887
nub>fat-HA	9.798 +- 1.779	16.425 +- 2.833	0.57	4.81E-06	0.875	0.726		

Figure 7

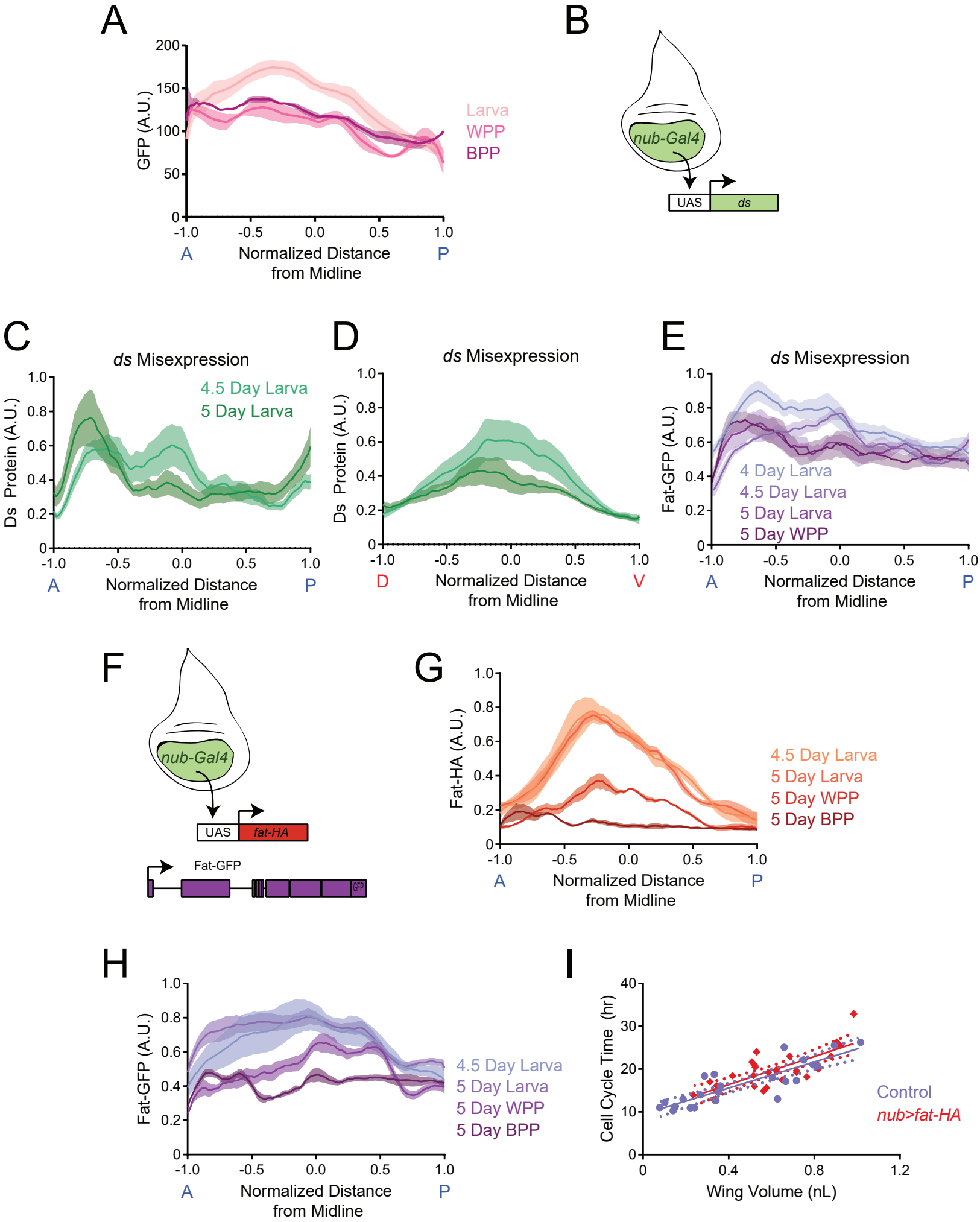
A
GFP (A.U.)
Larva
WPP
BPP
A
Normalized Distance from Midline
P
B
nub-Gal4
UAS
ds
C
ds Misexpression
Ds Protein (A.U.)
4.5 Day Larva
5 Day Larva
A
Normalized Distance from Midline
P
D
ds Misexpression
Ds Protein (A.U.)
D
Normalized Distance from Midline
V
E
ds Misexpression
Fat-GFP (A.U.)
4 Day Larva
4.5 Day Larva
5 Day Larva
5 Day WPP
A
Normalized Distance from Midline
P
F
nub-Gal4
UAS
fat-HA
Fat-GFP
GFP
G
Fat-HA (A.U.)
4.5 Day Larva
5 Day Larva
5 Day WPP
5 Day BPP
A
Normalized Distance from Midline
P
H
Fat-GFP (A.U.)
4.5 Day Larva
5 Day Larva
5 Day WPP
5 Day BPP
A
Normalized Distance from Midline
P
I
Cell Cycle Time (hr)
Control
nub>fat-HA
Wing Volume (nL)

Figure 7 - figure supplement 1

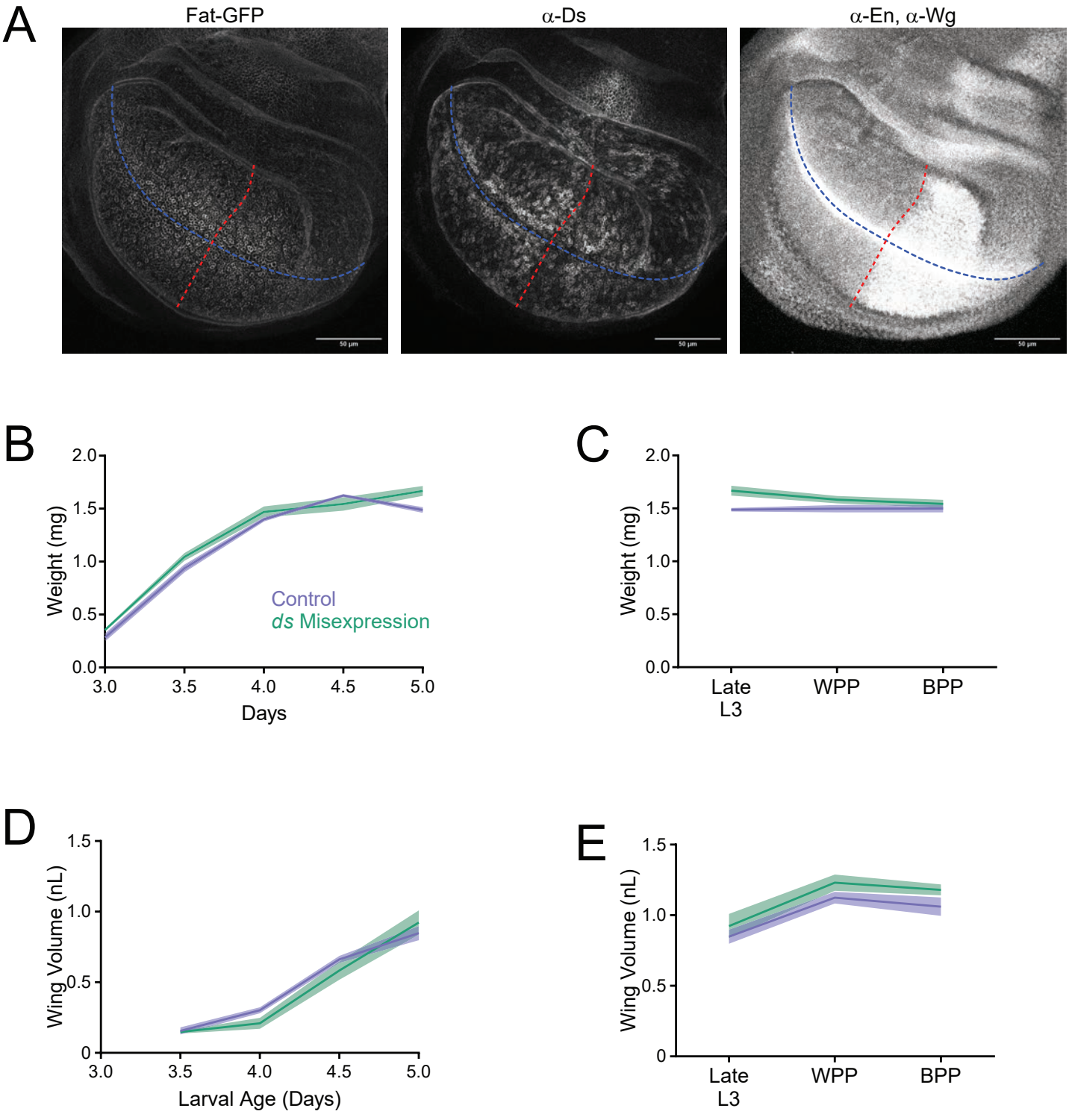
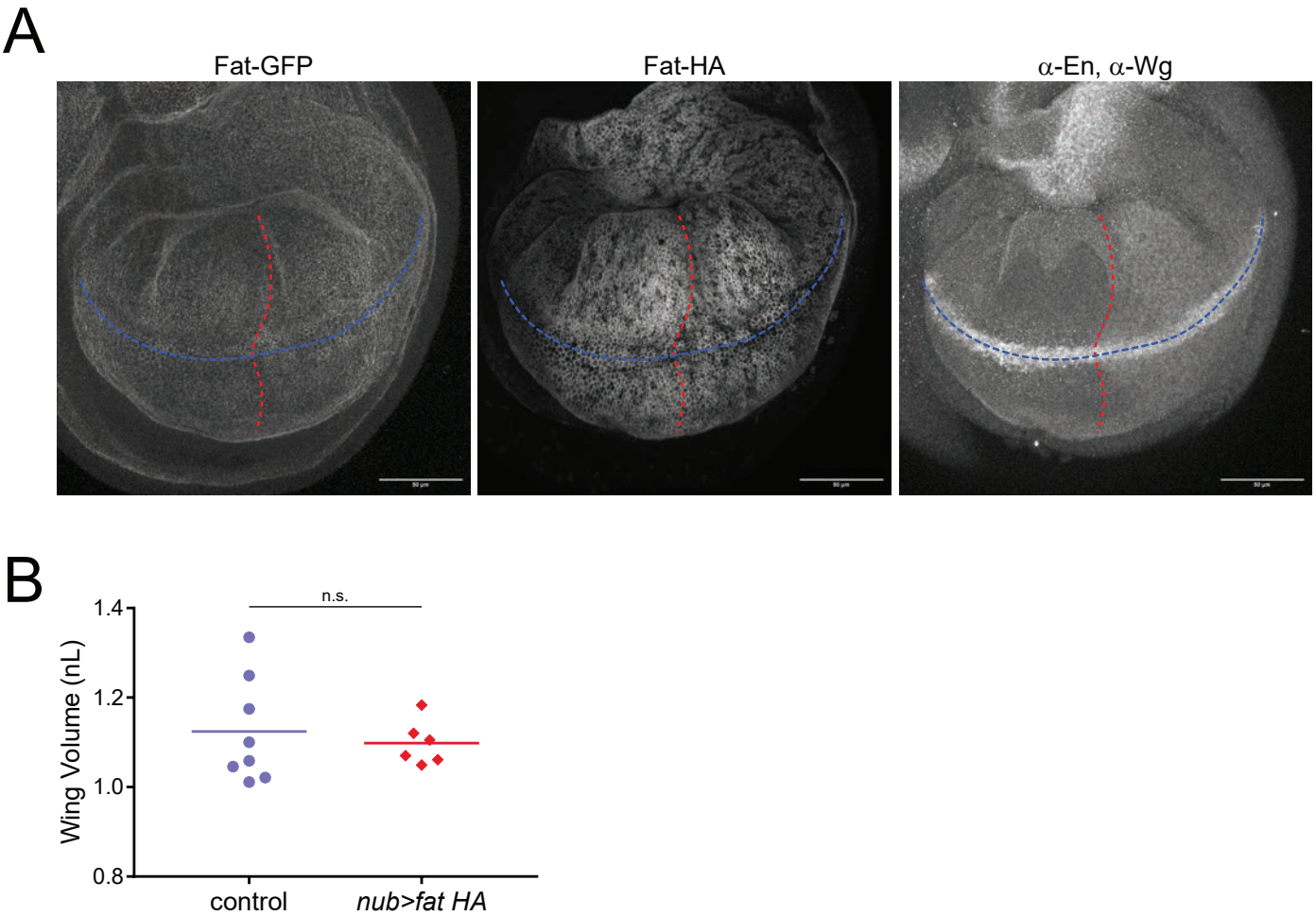
Figure 7 - figure supplement 2